SIAM J. NUMER. ANAL.
Vol. 43, No. 1, pp. 409–436

ANALYSIS OF FIRST-ORDER SYSTEM LEAST SQUARES (FOSLS) FOR ELLIPTIC PROBLEMS WITH DISCONTINUOUS COEFFICIENTS: PART II*

MARKUS BERNDT†, THOMAS A. MANTEUFFEL‡, AND STEPHEN F. MCCORMICK‡

Abstract. First-order system least squares (FOSLS) is a methodology that offers an alternative to standard methods for solving partial differential equations. This paper studies the first-order system least-squares approach for scalar second-order elliptic boundary value problems with discontinuous coefficients. In a companion paper [M. Berndt, T. A. Manteuffel, S. F. McCormick, and G. Starke, *Analysis of first-order system least squares (FOSLS) for elliptic problems with discontinuous coefficients: Part I*, SIAM J. Numer. Anal., 43 (2005), pp. 386–408], ellipticity of an appropriately scaled least-squares bilinear form is established in a natural norm. For some geometries this ellipticity is independent of the size of the jumps in the coefficients. The occurrence of singularities at interface corners, cross-points, reentrant corners, and irregular boundary points is discussed, and a basis of singular functions with local support around singular points is established. This paper describes a method for including discrete versions of the singular basis functions together with standard finite element spaces in a least-squares format at little additional computational cost. The singular basis functions are constructed to match the jump conditions that arise at interfaces between regions of continuity of the diffusion coefficient. Because these basis functions must be approximated in practice, the resulting discretization is by nature nonconforming. This necessitates the establishment here of a general error estimate for FOSLS L^2 minimization problems discretized by nonconforming finite elements. An advantage of the FOSLS formulation is that this estimate does not involve the consistency error term usually present in bounds for other methods. Based on this general estimate, error bounds are derived for the finite element space that includes singular basis functions. Numerical tests are included that confirm these discretization error bounds. Finally, a multilevel method is developed for solving the discrete system that uses singular basis functions on all levels, and its efficiency is demonstrated by the numerical results.

Key words. least-squares discretization, second-order elliptic problems, discontinuous coefficients, interface problems, singularities, finite elements, multilevel methods

AMS subject classifications. 65N55, 65N30, 65F10

DOI. 10.1137/S003614290342769X

1. Introduction.

In this paper we consider the application of first-order system least squares (FOSLS [11, 12]) to diffusion equations in the plane with jump-discontinuous coefficients:

$$\begin{aligned} -\nabla \cdot (a\nabla p) &= f \quad && \text{in } \Omega, \\ p &= g_D \quad && \text{on } \Gamma_D, \\ \mathbf{n} \cdot (a\nabla p) &= g_N \quad && \text{on } \Gamma_N. \end{aligned} \tag{1.1}$$

*Received by the editors May 7, 2003; accepted for publication (in revised form) August 31, 2004; published electronically June 14, 2005. This work was performed by an employee of the U.S. Government or under U.S. Government contract. The U.S. Government retains a nonexclusive, royalty-free license to publish or reproduce the published form of this contribution, or allow others to do so, for U.S. Government purposes. Copyright is owned by SIAM to the extent not limited by these rights.

http://www.siam.org/journals/sinum/43-1/42769.html

†Los Alamos National Laboratory, T-7, Mail Stop B284, Los Alamos, NM 87545 (berndt@lanl.gov). The research of this author was supported by the Department of Energy, under contract W-7405-ENG-36, LA-UR-02-3284.

‡Department of Applied Mathematics, Campus Box 526, University of Colorado at Boulder, Boulder, CO 80309-0526 (tmanteuf@boulder.colorado.edu, stevem@boulder.colorado.edu). The research of these authors was supported by the National Science Foundation under grant number DMS-8704169, and by the Department of Energy, Applied Math Program grant DE-FG03-94ER25217.

Here, $a > 0$ is a piecewise smooth function corresponding to some partition of domain $\Omega \subset \Re^2$, with boundary $\partial\Omega = \Gamma_D \cup \Gamma_N$ and outward unit normal $\mathbf{n}$, and the data f, g_D, and g_N are appropriately smooth functions. Our focus is on a two-stage FOSLS scheme whose primary aim is to approximate the flux $a\nabla p$.

Studies of the problem of accurate approximation of p by inclusion of special basis functions (cf. [30, 23]) and adaptive refinement (cf. [28]) has been extensive, but the development of efficient multilevel algorithms for the calculation of stress intensity factors is lagging. The only example we are aware of is the full multigrid algorithm for interface problems stemming from cracks, introduced in [7, 9].

The least-squares methodology for systems of first order is by now several decades old and had its first applications in continuum mechanics (see, for example, [20, 32, 21, 25, 15, 22]). Only fairly recently has it produced H^1-equivalent forms to which optimal multigrid solvers have been applied (see, for example, [12]). For a thorough review of the least-squares methodology, see [4] and the references therein.

In the FOSLS formulations developed in [11, 12], the aim was to rewrite the original scalar equation as a first-order system in such a way that its associated least-squares functional has an H^1-equivalent homogeneous part. This equivalence enables simpler finite element discretization methods and ensures that the resulting discrete problem can be solved efficiently by a standard multigrid method. However, because we allow discontinuities in a here, the flux is discontinuous across interfaces and may be singular at some points in the domain. We are therefore led to the development of a special FOSLS L^2 approach for solving (1.1).

In this paper we develop a flux-only FOSLS functional that is continuous and coercive in a scaled space, $H(\operatorname{div} a, \Omega) \cap H(\operatorname{curl} a, \Omega)$, which we denote as $\mathbf{W}$ (see section 2). We denote the space of piecewise H^1 vector valued functions as $H^1_S(\Omega)$ (see section 4). In [2] it was shown that $H^1_S(\Omega) \cap \mathbf{W}$ has finite codimension in $\mathbf{W}$. The singular basis functions, together with $H^1_S(\Omega)\mathbf{W}$, span $\mathbf{W}$ (cf. [2]).

The basic idea behind our special FOSLS scheme is to include singular basis functions in the finite element space and thus accurately model the singular behavior of the flux. These basis functions are constructed so that their action in the weak form involves integration only inside a small fringe region around the singularity. Thus, the additional cost is minimal, yet optimal accuracy is retained.

Alternatives to the approach we develop here are described in detail in [2] and include adding H^1 singular basis functions in standard Galerkin methods to enhance the rate of convergence (cf. [30, 17, 7, 10]) and the use of $H(\operatorname{div})$ conforming finite element spaces with mixed formulations (see [8]) or with FOSLS functionals that are based on $H(\operatorname{div})$ (see [11, 26, 27]). Standard finite element spaces can be used with FOSLS functionals that are weighted to eliminate the overall impact on accuracy of the singular behavior of the flux [18, 17, 24]. Unfortunately, this weighting approach does not provide accurate resolution of the solution close to singularities of the flux, which is the main objective of the approach developed here.

Other alternatives use FOSLS based on inverse norms [6, 5, 13, 3] and FOSLS* [14]. The FOSLS L^2 approach developed here achieves accuracy in the stronger H^1-like norm, which may be preferred in many practical cases.

To estimate discretization accuracy for our special FOSLS scheme, we derive a general error bound for L^2-type FOSLS discretized by nonconforming finite elements. Similar nonconforming estimates for other methods typically involve consistency error terms (cf. [1]), but they are not needed in the FOSLS context. This special property of FOSLS is important because it means that error estimates for nonconforming finite

elements may be derived solely from relatively simple interpolation error bounds.

The FOSLS reformulation of (1.1) is derived in section 2. In section 3, the calculation of exponents of singular basis functions is described, and, in section 4, we describe the finite element discretization scheme, complete with singular basis functions. In section 5, the general nonconforming error bound is derived and applied to estimating the accuracy of our augmented basis approach. These estimates are confirmed by the numerical results at the end of section 5. We introduce a multilevel solver in section 6 that is based on coarsening with singular basis functions on all levels. The W-cycle form of this algorithm exhibits typical multigrid convergence behavior, as the numerical results of section 7 also confirm.

2. Problem statement and FOSLS formulation. Assume that $\Omega \subset \Re^2$ is a simply connected polygonal region and that

$$\overline{\Omega} = \bigcup_{j=1}^{J} \overline{\Omega}_j, \tag{2.1}$$

where Ω_j are mutually disjoint open simply connected polygonal regions. Assume also that $\partial\Omega = \Gamma_D \cup \Gamma_N$, Γ_D has positive measure, and Γ_D and Γ_N both consist of a finite number of connected pieces. The case in which $\Gamma_D = \emptyset$ is a simple extension.

Consider the following div-curl first-order system for the scaled flux $\mathbf{u} := \sqrt{a}\nabla p$:

$$\begin{aligned} -\nabla \cdot (\sqrt{a}\mathbf{u}) &= f \quad \text{in } \Omega, \\ \nabla \times (\mathbf{u}/\sqrt{a}) &= 0 \quad \text{in } \Omega, \\ \mathbf{n} \cdot (\sqrt{a}\mathbf{u}) &= 0 \quad \text{on } \Gamma_N, \\ \mathbf{n} \times (\mathbf{u}/\sqrt{a}) &= 0 \quad \text{on } \Gamma_D. \end{aligned} \tag{2.2}$$

(We treat the homogeneous boundary condition case for simplicity. The general case of nonzero g_N and $g_D := \mathbf{n} \times \nabla p$ could be treated by standard lifting or superposition techniques.)

Under the additional smoothness assumptions $a \in C^{1,1}(\Omega)$, $f \in L^2(\Omega)$, and in the absence of reentrant corners and boundary points in which Γ_D and Γ_N meet with interior angle greater than $\pi/2$, we can assert the following [12]: scalar equation (1.1) has a unique solution $p \in H^2(\Omega)$; system (2.2) has a unique solution $\mathbf{u} \in H^1(\Omega)^2$; and the two problems are equivalent in the sense that their solutions correspond according to the relation $\mathbf{u} := \sqrt{a}\nabla p$.

We are interested here in the discontinuous coefficient case, where a is assumed only to be piecewise continuous. Theoretical properties of the first-order system and the corresponding FOSLS functional for this case are studied in the companion paper [2]. In the present paper, we focus on the discretization and multilevel solver for the discrete problem. Problems with reentrant corners and irregular boundary points can be handled in an analogous manner and are omitted for simplicity of presentation.

System (2.2) gives rise to the scaled least-squares functional

$$\mathcal{G}(\mathbf{u}; f) = \left\| (1/\sqrt{a})\nabla \cdot (\sqrt{a}\mathbf{u} + f) \right\|_0^2 + \left\| \sqrt{a}\nabla \times (\mathbf{u}/\sqrt{a}) \right\|_0^2 \tag{2.3}$$

and the associated FOSLS L^2 minimization problem

$$\mathbf{u} = \arg \min_{\mathbf{v} \in \mathbf{W}} \mathcal{G}(\mathbf{v}; f), \tag{2.4}$$

which is well posed on the space

$$\mathbf{W} = \{\mathbf{v} \in H(\operatorname{div} a, \Omega) \cap H(\operatorname{curl} a, \Omega) : \mathbf{n} \cdot (\sqrt{a}\mathbf{v}) = 0 \operatorname{on} \Gamma_N, \mathbf{n} \times (\mathbf{v}/\sqrt{a}) = 0 \text{ on } \Gamma_D\}, \tag{2.5}$$

where

$$H(\operatorname{div} a, \Omega) = \left\{\mathbf{v} \in L^2(\Omega)^2 : \nabla \cdot (\sqrt{a}\mathbf{v}) \in L^2(\Omega)\right\},$$
$$H(\operatorname{curl} a, \Omega) = \left\{\mathbf{v} \in L^2(\Omega)^2 : \nabla \times (\mathbf{v}/\sqrt{a}) \in L^2(\Omega)\right\}.$$

We equip $\mathbf{W}$ with the seminorm

$$|\mathbf{u}|_{\mathbf{W}} = \left\|(1/\sqrt{a})\nabla \cdot (\sqrt{a}\mathbf{u})\right\|_0^2 + \left\|\sqrt{a}\nabla \times (\mathbf{u}/\sqrt{a})\right\|_0^2.$$

Note that this is actually a norm because of the assumption that Γ_D has positive measure (see [2, Lemma 3.3]). Note also that $\mathcal{G}$ is trivially $\mathbf{W}$ elliptic in the sense that

$$\mathcal{G}(\mathbf{u}; 0) = |\mathbf{u}|_{\mathbf{W}}^2. \tag{2.6}$$

Minimization problem (2.4) leads to the following variational problem: find $\mathbf{u} \in \mathbf{W}$ such that

$$\mathcal{F}(\mathbf{u}, \mathbf{v}) = \left\langle f/a, \nabla \cdot (\sqrt{a}\mathbf{v})\right\rangle_{0,\Omega} \tag{2.7}$$

for all $\mathbf{v} \in \mathbf{W}$, with

$$\mathcal{F}(\mathbf{u}, \mathbf{v}) = \left\langle (1/a)\nabla \cdot (\sqrt{a}\mathbf{u}), \nabla \cdot (\sqrt{a}\mathbf{v})\right\rangle_{0,\Omega} + \left\langle a\nabla \times (\mathbf{u}/\sqrt{a}), \nabla \times (\mathbf{v}/\sqrt{a})\right\rangle_{0,\Omega}.$$

Suppose that a is piecewise continuous with respect to the partitioning (2.1) of Ω in the maximal sense; that is, a is continuous on Ω_j and no open set $\mathcal{O}_j \supset \Omega_j$ exists for which $a|_{\mathcal{O}_j}$ is continuous, $1 \le j \le J$. Under these assumptions, variational problem (2.7) has a unique solution in $\mathbf{W}$ that is also the unique solution of FOSLS minimization problem (2.4) (see [2]).

An edge that lies in the intersection of the closure of two subdomains is called an interface. Points where two interfaces meet are called cross-points. Cross-points, reentrant corners, and irregular boundary points are all potential singular points. Now, the solution $\mathbf{u} \in \mathbf{W}$ of problem (2.2) satisfies certain conditions across the interfaces. Denote by $\mathbf{n}_{\mathcal{I}}$ a unit vector normal to interface $\mathcal{I}$. Then

$$\mathbf{n}_{\mathcal{I}} \cdot (\sqrt{a}\mathbf{u}) \text{ and } \boldsymbol{\tau}_{\mathcal{I}} \cdot (\mathbf{u}/\sqrt{a}) \text{ are continuous a.e. across interfaces.} \tag{2.8}$$

These interface conditions must be true in order for the first two equations in (2.2) to make sense. For the first condition in (2.8) see, for example, [33, Chapter 6.2]. The second condition can be derived analogously.

3. Approximation of singularities. In [2, section 5], a splitting of $\mathbf{W}$ into a finite-dimensional space spanned by singular functions and locally smooth functions is introduced. This leads to a decomposition of any $\mathbf{u} \in \mathbf{W}$ as

$$\mathbf{u} = \mathbf{u}_0 + \sum_{m=1}^{M} \sum_{n=1}^{N_m} \omega_m \delta_m \mathbf{s}_{m,n}, \tag{3.1}$$

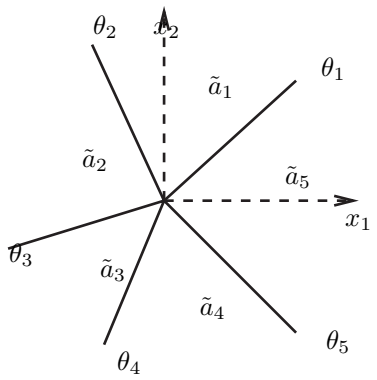

FIG. 3.1. *Cross-point,* $I = 5$.

where $\mathbf{u}_0|_{\Omega_i} \in H^1(\Omega_i)$, δ_m is a cut-off function at a singular point (see Figure 4.2 for an example), and $\mathbf{s}_{m,n}$, $n = 1, \ldots, N_m$, are the singular functions associated with singular point $\mathbf{x}_m$, $m = 1, \ldots, M$. In this paper, our focus is on singular points that are cross-points (see Figure 3.1 for an example). The other types of singular points, described in [2, section 5], can be treated in an analogous fashion.

The exact nature of a singularity at a cross-point can be calculated using a and the geometry of interfaces in the neighborhood of the cross-point. To obtain a simple representation of such singularities (see [23] and [30]), additional constraints on the behavior of a within Ω_i are necessary. We first summarize the results of [2, section 5] and then proceed to describe the numerical method that is used to calculate singular basis functions.

Given a polar coordinate system (r, θ), centered at a cross-point, we recall that $a \in C^{1,1}(\Omega_i)$, for each subdomain Ω_i, and assume that a satisfies

$$\lim_{r\to 0} a_\theta = 0, \qquad \lim_{r\to 0} r a_r = 0. \tag{3.2}$$

The task of finding a representation for the singularity at a cross-point reduces to finding solutions of the Sturm–Liouville eigenvalue problem (see [2, section 5] for a detailed derivation)

$$-(\tilde{a}T')' = \tilde{a}\alpha^2 T \ \text{ on } \ [0, 2\pi), \tag{3.3}$$

where $\tilde{a}_i = \lim_{r\to 0} a(r, \theta)$ in Ω_i.

Each interface that adjoins the cross-point is characterized by the angle of its tangent at the cross-point with the x_1-axis. Denote by I the number of interfaces adjoining at a given cross-point, and by θ_i, $i = 1, \ldots, I$, the angles their tangents make with the x_1-axis (see Figure 3.1 for an example with $I = 5$). Assume that these interface angles are ordered such that $\theta_i < \theta_{i+1}$, $i = 1, \ldots, I-1$. Let $\theta_{I+1} = \theta_1$.

Eigenfunctions of (3.3) have the form

$$T_n(\theta) = \lambda_{n,i} \cos(\alpha_n \theta) + \mu_{n,i} \sin(\alpha_n \theta), \tag{3.4}$$

for $\theta \in (\theta_i, \theta_{i+1})$, where α_n^2 is the associated eigenvalue. According to [2, Theorem 5.1], we must calculate all eigenvalues $0 < \alpha_n^2 < 1$ and associated eigenfunctions of (3.3),

to obtain all singular functions

(3.5)
$$\mathbf{s}_{m,n} = \sqrt{a}\nabla r^{\alpha_n} T_n(\theta) = \sqrt{a}\alpha_n r^{\alpha_n - 1} \begin{pmatrix} \lambda_{ni}\sin((\alpha_n - 1)\theta) + \mu_{ni}\cos((\alpha_n - 1)\theta) \\ \lambda_{ni}\cos((\alpha_n - 1)\theta) - \mu_{ni}\sin((\alpha_n - 1)\theta) \end{pmatrix},$$

for $\theta \in (\theta_i, \theta_{i+1})$, where λ_{ni} and μ_{ni} are constant inside each Ω_i. Note also that $\mathbf{s}_{m,n} = \sqrt{a}\nabla\sigma_n$ with

$$\sigma_n(r,\theta) = r^{\alpha_n}(\lambda_{ni}\sin\alpha_n\theta + \mu_{ni}\cos\alpha_n\theta) \quad \text{for} \quad \theta \in (\theta_i, \theta_{i+1}). \tag{3.6}$$

Remark 1. In [2], a representation of the singular functions is used that differs slightly from (3.5). It is easy to show that the two representations are equivalent.

For convenience we will now drop the subscript n where the meaning is apparent. The exponent α and the coefficients (λ_i, μ_i) can be determined by enforcing continuity of both $T(\theta)$ and $\tilde{a}T'(\theta)$ across interfaces. To obtain first approximations to the eigenvalues α^2, we discretize eigenvalue problem (3.3) and solve the resulting algebraic generalized eigenvalue problem. Note that we are primarily interested in the smallest values of α^2, that is, $0 \le \alpha^2 \le 1$. The eigenvectors associated with these small eigenvalues are well approximated using a fairly coarse discretization. Values of α that are obtained in this way are used as starting values of a secant iteration that is based on the following idea.

Interface conditions (2.8) give rise to a $2I \times 2I$ nonlinear system of equations for α, λ_i, and μ_i, $i = 1, \ldots, I$, which can be written in the compact form

$$M(\alpha)(\lambda_1, \mu_1, \ldots, \lambda_I, \mu_I)^t = \underline{0}. \tag{3.7}$$

A nontrivial solution exists only when $M(\alpha)$ is singular, that is, when $\det M(\alpha) = 0$. To find roots of $\det M(\alpha)$, we use a secant iteration with starting values obtained from the solution of the discretized Sturm–Liouville eigenvalue discussed in above.

Suppose we compute an approximation $\tilde{\alpha} = \alpha + \eta$. To estimate η, we find $\underline{x}$ that has norm one and minimizes $\|M(\tilde{\alpha})\underline{x}\|$. Thus, $\underline{x}$ is a right singular vector of $M(\tilde{\alpha})$ and $\|M(\tilde{\alpha})\underline{x}\| = \sigma_n$, the smallest singular value of $M(\tilde{\alpha})$, which is easily computed because $M(\tilde{\alpha})$ is of small dimension. Moreover,

$$M(\tilde{\alpha})\underline{x} = \sigma_n \underline{r}, \tag{3.8}$$

where $\underline{r}$ is the left singular vector of $M(\tilde{\alpha})$ and $\|\underline{r}\| = 1$.

Let α be the exact value, and let the inexact $\tilde{\alpha} = \alpha + \eta$. Then we have the matrix expansion

$$M(\alpha + \eta) = M(\alpha) + \eta M'(\alpha + \hat{\eta}) \simeq M(\alpha) + \eta M'(\alpha + \eta),$$

where $\hat{\eta} \in (0, \eta)$. We can easily compute $M'(\alpha + \eta)$. Since $M(\alpha)$ is singular, we know that the distance from $M(\alpha + \eta)$ to $M(\alpha)$ in the Frobenius norm is larger than the smallest singular value of $M(\alpha + \eta)$; that is,

$$\sigma_n \le \|M(\alpha + \eta) - M(\alpha)||_F \simeq \eta\|M'(\alpha + \eta)\|_F.$$

Thus, we get a lower bound on η. Conversely, we see that as $\eta \to 0$, we can get a bound on $\sigma_n \to 0$.

In conclusion, the coefficients become accurate at the same rate as alpha becomes accurate. Also, we can determine an approximate lower bound on the accuracy of

alpha by computing the singular values of $M(\tilde{\alpha})$. If the error in alpha is too big, we do more computational work. (In [2, (5.12)], $M(\alpha)$ is scaled such that the dependence on a is lumped into 2×2 block diagonal terms D_i that have no dependence on α but depend on the ratio a_i/a_{i-1}. In this paper, we use a slightly different scaling, where $D_i = \mathrm{diag}(a_{i-1}, -a_i)$.)

The calculations that are described in this section are not very costly, since typically, the number of interfaces adjoining a cross-point is very small, and the number of eigenvalues of the Sturm–Liouville problem (3.3) in which we are interested is of order $O(1)$ (see [23]).

4. Finite element discretization. For simplicity, we have assumed that domain Ω and its subdomains Ω_j are polygonal, which allows the geometry of the discontinuities of a to be resolved exactly using a triangular mesh. Let $\mathcal{T}_h$ be a quasiuniform triangulation (see, for example, [8, Definition 4.4.13]) constructed so that no element cuts across any interface (i.e., each element is contained in just one subdomain). Our discretization method is based on the decomposition introduced in [2] that isolates the singular functions from the piecewise H^1 functions. To this end, let $\delta_m \in H^1(\Omega)$ denote any given"cut-off" function that has value one in a small area about cross-point m and values that taper to 0 in a small outer "fringe," $1 \le m \le M$. (See Figure 4.2.) Let $\mathbf{s}_{m,n}$ be the nth singular basis function at cross-point m, $1 \le n \le N_m, 1 \le m \le M$. Then $\delta_m \mathbf{s}_{m,n} \in W$, provided that δ_m has support inside Ω and all interfaces inside the fringe and platform of δ_m are straight lines. We will be more specific about $\mathbf{s}_{m,n}$ below. Defining the "split" space of piecewise H^1 functions by

$$H^1_S(\Omega) := \left\{ \mathbf{u} \in (L^2(\Omega))^2 \ : \ \mathbf{u}|_{\Omega_j} \in (H^1(\Omega_j))^2, \ j = 1, \ldots, J \right\} \tag{4.1}$$

and letting $\mathbf{W}^1_S := \mathbf{W} \cap H^1_S(\Omega)$, then our decomposition is given by

$$\mathbf{W} = \mathbf{W}^1_S \ \oplus \ \mathrm{span}\left\{ \delta_m \mathbf{s}_{m,n} : 1 \le m \le M, 1 \le n \le N_m \right\}, \tag{4.2}$$

(cf. [2], Theorem 5.1). At interior nodes of the subdomains Ω_j, we use standard piecewise linear nodal basis functions, whose coefficients at the nodal values are the unknowns. (We will add certain quadratic basis functions shortly.) For vertices that lie on interfaces, we use piecewise linear basis functions that satisfy interface conditions (2.8) exactly and are scaled to have a maximum of one (see also Figure 4.1).

Singular components $\delta_m \mathbf{s}_{m,n}$ are discretized by choosing a discrete cut-off function $\delta_m = \delta^h_m$ and replacing $\mathbf{s}_{m,n}$ by a discrete approximation $\tilde{\mathbf{s}}_{m,n}$, as described in section 3. Each cross-point m is surrounded by the support of its cut-off function,

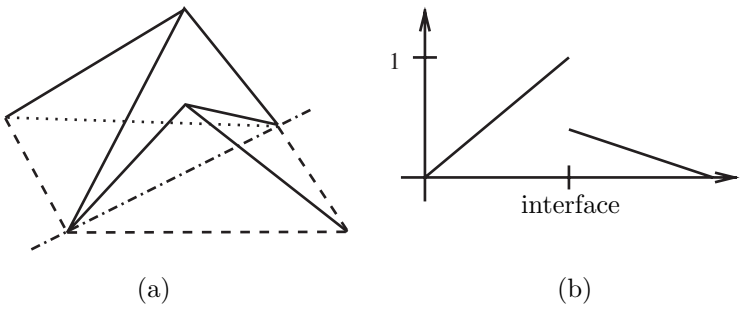

FIG. 4.1. *A discontinuous linear basis function in 3D view* (a) *and in side view* (b).

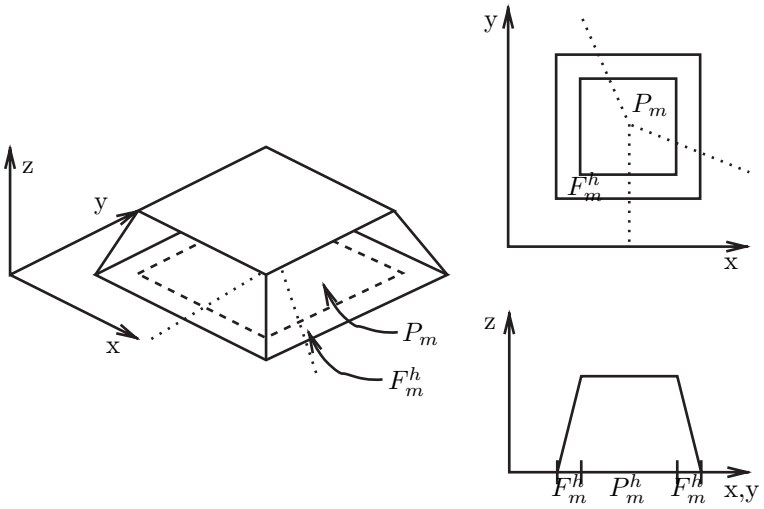

FIG. 4.2. *The cut-off function δ_m^h centered at a cross-point (P_m = platform, F_m^h = fringe, dotted lines are interfaces).*

which consists of a platform P_m and outer fringe F_m^h consisting of one outer ring of level h triangles. The platform also consists of level h triangles, but it is otherwise fixed in size. The supports $P_m \cup F_m^h$ are constructed at each cross-point to be large enough to obtain a reasonable approximation to the singular functions but small enough to ensure that they do not intersect with each other. Cut-off function δ_m^h is then defined so that $\delta_m^h|_\tau$ is linear for all $\tau \subset F_m^h$ and has value 1 inside its platform. See Figure 4.2.

Denoting by $\mathcal{F}_\tau(\cdot,\cdot)$ the $\mathcal{F}$ inner product evaluated on the element τ, we have

$$\mathcal{F}_\tau(\delta_m^h \mathbf{s}_{m,n}, \mathbf{v}) = 0 \quad \text{for all} \quad \tau \in P_m,$$

since $\delta_m^h = 1$ inside P_m. This implies that, for elements inside the platforms, entries in element stiffness matrices that involve singular basis functions are zero. Only elements in the fringes have element stiffness matrices that have contributions from integration of singular basis functions. To evaluate these fringe integral terms, we use two-dimensional Gaussian quadrature of order high enough to ensure that it does not corrupt the discretization error estimates we obtain in the following sections. (Recall that the singular functions are smooth in the fringe.) Outside platforms and fringes, there are no contributions from singular basis functions. In conclusion, each singular basis function need only be numerically integrated on the small number of elements that comprise the fringe of its cut-off function.

To control the computational work of integrating the singular basis functions, we have limited the fringes to width h, which reduces discretization accuracy. To avoid this loss, we introduce quadratic "bubble-like" basis functions in the fringes, with supports consisting of two triangles that share an edge within the fringe. Within each triangle, the quadratic function is defined to be the product of a linear function that is zero on one of the nonshared edges and another that is zero on the other nonshared edge. When the triangle pair is in a single Ω_j, the basis function is scaled to be 1 at the midpoint of the shared edge (see Figure 4.3(c)). If, instead, the edge coincides with an interface, the discontinuous basis function is such that it satisfies the interface

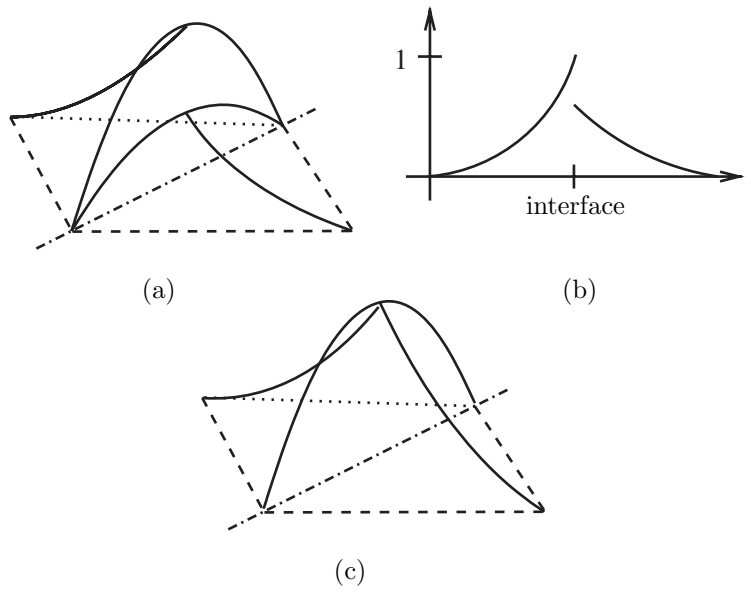

FIG. 4.3. *A discontinuous quadratic basis function in* 3*D view* (a) *and in side view* (b); *a continuous quadratic basis function* (c).

conditions (2.8) exactly and has a maximum of one. See Figure 4.3(a) and (b) for a schematic.

In the next section, we derive an error estimate that illustrates the necessity for such an increase in discretization order inside the fringes (see the proof of Theorem 5.1).

Our discretization is, thus, defined by the space $\mathbf{W}^h$ of elements of the form

$$\mathbf{u}^h = \mathbf{u}_L^h + \mathbf{u}_Q^h + \sum_{m=1}^{M} \sum_{n=1}^{N_m} \omega_{m,n} \delta_m^h \tilde{\mathbf{s}}_{m,n}, \tag{4.3}$$

where is $\mathbf{u}_L^h$ is piecewise linear (with respect to $\mathcal{T}^h$) and continuous in Ω_j, $\mathbf{u}_Q^h$ is piecewise quadratic and continuous in Ω_j but with support contained in the fringe, and $\tilde{\mathbf{s}}_{m,n}$ is an approximation to $\mathbf{s}_{m,n}$. The discrete problem corresponding to (2.7) is then as follows: Find $\mathbf{v}^h \in \mathbf{W}^h$ such that

$$\mathcal{F}(\mathbf{u}^h, \mathbf{v}^h) = \left\langle f/a, \nabla \cdot (\sqrt{a}\mathbf{v}^h) \right\rangle_{0,\Omega} \tag{4.4}$$

for all $\mathbf{v}^h \in \mathbf{W}^h$.

Both $\mathbf{u}_L^h$ and $\mathbf{u}_Q^h$ satisfy the interface conditions exactly, but the singular function approximations $\tilde{\mathbf{s}}_{m,n}$ do not, because $\tilde{\alpha}$ is not exact. This means that the discrete space is generally nonconforming: $\mathbf{W}^h \not\subset \mathbf{W}$. Thus, standard theory for discretization accuracy does not apply, and we are left to develop our own estimates.

5. Error estimates. We begin by establishing an error estimate for the case of a conforming subspace, where the singular basis functions are assumed to be known exactly. To cover the practical case, where approximate singular basis functions are used, we then derive a general error estimate for FOSLS L^2 formulations with nonconforming finite elements and apply it to the case of nonconforming singular basis functions.

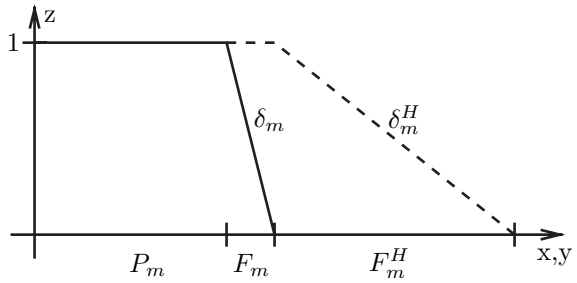

FIG. 5.1. *Side view of cut-off functions δ_m^h and δ_m^H.*

5.1. The conforming case: $\mathbf{W}^h \subset \mathbf{W}$. Let $2H_m$ be less than the shortest distance from P_m to the nearest other platform or boundary. Let F_m^H be a fringe of width H_m, and let δ_m^H be the associated cut-off function (see Figure 5.1). Using the decomposition of $\mathbf{W}$ given in (4.2), write the solution of variational problem (4.4) as

$$\mathbf{u} = \mathbf{u}_0 + \sum_{m=1}^{M} \sum_{n=1}^{N} \omega_{m,n} \delta_m^H \mathbf{s}_{m,n}, \tag{5.1}$$

where $\mathbf{u}_0 \in \mathbf{W}_S^1$. Now we state the error estimate for the conforming case.

THEOREM 5.1 (estimate for conforming $\mathbf{W}^h$). *Assume that $\mathbf{W}^h \subset \mathbf{W}$. Let $\mathbf{u} \in \mathbf{W}$ denote the solution of variational problem* (2.7) *and $\mathbf{u}^h \in \mathbf{W}^h$ the solution of discrete variational problem* (4.4). *Let $2H_m$ be less than the distance between P_m and the closest other platform or boundary, and assume that $0 < h < H_m$, for $m = 1, \ldots, M$. Then*

$$\left|\mathbf{u} - \mathbf{u}^h\right|_{\mathbf{W}} \leq C_1 h^{\sigma-1} \left|\mathbf{u}_0\right|_{\sigma,S} + C_2 h \sup_{m,n} |\omega_{m,n}|, \tag{5.2}$$

where $\sigma \in (1, 2]$ depends on the smoothness of $\mathbf{u}_0$, $\omega_{m,n}$ are the coefficients in (5.1), *and the constants $C_1, C_2 > 0$ are independent of h.*

Proof. Since $\mathbf{W}^h \subset \mathbf{W}$, then by (4.4), $\mathbf{u}^h$ satisfies

$$\left|\mathbf{u} - \mathbf{u}^h\right|_{\mathbf{W}} = \inf_{\mathbf{v}^h \in \mathbf{W}^h} \left|\mathbf{u} - \mathbf{v}^h\right|_{\mathbf{W}} \leq \left|\mathbf{u} - \mathbf{w}^h\right|_{\mathbf{W}}, \tag{5.3}$$

for any particular $\mathbf{w}^h \in \mathbf{W}^h$. As in (5.1), denote by δ_m^H the cut-off function that is one in $P_m \cup F_m$ and drops to zero linearly in the extended fringe F_m^H around $P_m \cup F_m^h$ of width H_m. See Figure 5.1 for a side view of this function. Note that all F_m^H, $m = 1, \ldots, M$, are mutually disjoint. Let $I^h : C(\Omega) \to \mathbf{W}$ denote a linear nodal interpolant operator outside $\bigcup_{m=1}^M F_m^h$ and a quadratic nodal interpolant operator in $\bigcup_{m=1}^M F_m^h$. Coefficients of linear basis functions are obtained by function evaluation at their vertex, whereas coefficients of quadratic basis functions are obtained by evaluating the difference of the function itself and the linear interpolant. We now write

$$\mathbf{u} = \mathbf{u}_0 + \sum_{m=1}^{M} \sum_{n=1}^{N_m} \omega_{m,n} (\delta_m^H - \delta_m^h) \mathbf{s}_{m,n} + \sum_{m=1}^{M} \sum_{n=1}^{N_m} \omega_{m,n} \delta_m^h \mathbf{s}_{m,n}, \tag{5.4}$$

where $\mathbf{u}_0 \in \mathbf{W}_S^1$ does not depend on h. Define

$$\mathbf{w}^h := I^h\left(\mathbf{u}_0 + \sum_{m=1}^{M}\sum_{n=1}^{N_m}\omega_{m,n}\psi_m\mathbf{s}_{m,n}\right) + \sum_{m=1}^{M}\sum_{n=1}^{N_m}\omega_{m,n}\delta_m^h\mathbf{s}_{m,n}, \tag{5.5}$$

where $\psi_m := \delta_m^H - \delta_m^h$. Substituting (5.4) and (5.5) into (5.3) and using the triangle inequality, we obtain

$$\left|\mathbf{u}-\mathbf{w}^h\right|_{\mathbf{W}} \le \left|\mathbf{u}_0 - I^h\mathbf{u}_0\right|_{\mathbf{W}} + \sum_{m=1}^{M}\sum_{n=1}^{N_m}|\omega_{m,n}|\left|\psi_m\mathbf{s}_{m,n} - I^h\psi_m\mathbf{s}_{m,n}\right|_{\mathbf{W}}. \tag{5.6}$$

Since $\mathbf{u}_0 \in \mathbf{W}_S^1$ does not depend on h, we can use [19, Theorem 4.4.20] to estimate the first term in (5.6):

$$\left|\mathbf{u}_0 - I^h\mathbf{u}_0\right|_{\mathbf{W}} = \left|\mathbf{u}_0 - I^h\mathbf{u}_0\right|_{1,S} \le \tilde{C}_1 h^{\sigma-1}\left|\mathbf{u}_0\right|_{\sigma,S}. \tag{5.7}$$

Here, $1 < \sigma \le 2$ depends on the smoothness of $\mathbf{u}_0$.

Since $\psi_m s_{m,n} \in \mathbf{W}_S^1$, we have

$$\left|(I-I^h)\psi_m s_{m,n}\right|_{\mathbf{W}}^2 \le \sum_{\tau\in F_m^h}\left|(I-I^h)\psi_m s_{m,n}\right|_{1,\tau}^2 + \sum_{\tau\in F_m^H\setminus F_m^h}\left|(I-I^h)\psi_m s_{m,n}\right|_{1,\tau}^2.$$

Since the finite element space includes quadratics on F_m^h, the two terms on the right-hand side satisfy

$$\left|(I-I^h)\psi_m s_{m,n}\right|_{1,\tau} \le \begin{cases} ch^2\|\psi_m s_{m,n}\|_{3,\tau} & \text{for } \tau \in F_m^h, \\ ch\|\psi_m s_{m,n}\|_{2,\tau} & \text{for } \tau \in F_m^H\setminus F_m^h. \end{cases}$$

Using the inverse inequality and noting that ψ is linear, we have

$$\|\psi_m s_{m,n}\|_{3,\tau} \le \frac{c}{h}\|s_{m,n}\|_{3,\tau} \qquad \text{for } \tau \in F_m^h$$

and

$$\|\psi_m s_{m,n}\|_{2,\tau} \le \frac{c}{H_m}\|s_{m,n}\|_{2,\tau} \qquad \text{for } \tau \in F_m^H\setminus F_m^h.$$

Putting this all together, we have

$$\left|(I-I^h)\psi_m s_{m,n}\right|_{\mathbf{W}}^2 \le ch^2\|s_{m,n}\|_{3,F_m^h}^2 + \frac{c}{H_m}h^2\|s_{m,n}\|_{2,F_m^H}^2. \tag{5.8}$$

Now, using (5.8) and (5.7) in (5.6), we obtain the estimate

$$\left|\mathbf{u}-\mathbf{w}^h\right|_{\mathbf{W}} \le \tilde{C}_1 h^{\sigma-1}\left|\mathbf{u}_0\right|_{\sigma,S} + h\sum_{m=1}^{M}C_m\sum_{n=1}^{N_m}|\omega_{m,n}|\,\|\mathbf{s}_{m,n}\|_{3,S,F_m^H} \tag{5.9}$$

$$\le C_1 h^{\sigma-1}\left|\mathbf{u}_0\right|_{\sigma,S} + C_2 h\sup_{m,n}|\omega_{m,n}|. \tag{5.10}$$

This completes the proof. ∎

Remark 2. If the right-hand side of (2.2) is sufficiently smooth, then adding all singular functions of the form (3.5) to the finite element space for which $\alpha_n \in (0,2]$ yields a bound of $O(h)$ in (5.2) (see [7]).

In practice, subspace $\mathbf{W}^h$ contains only approximate singular basis functions, which implies $\mathbf{W}^h \not\subset \mathbf{W}$. In the next section, we derive an error estimate for a general nonconforming finite element space that is used in section 5.3.

5.2. A general error estimate for FOSLS L^2 formulations with nonconforming finite elements. In this section, we depart from the framework and notation that were introduced in the previous section. We introduce a general methodology for derivation of error estimates for FOSLS L^2 formulations that use nonconforming finite element spaces. First consider a general FOSLS L^2 functional

$$\mathcal{G}(\mathbf{u};\mathbf{f}) := \|\mathcal{L}\mathbf{u}-\mathbf{f}\|_{0,\Omega}^2\,, \tag{5.11}$$

where Ω is a bounded open domain, $\mathbf{u}$ an element of a Hilbert space $\boldsymbol{\mathcal{W}}$, $\mathbf{f}\in(L^2(\Omega))^k$, and $\mathcal{L}$ a first-order differential operator. This gives rise to the FOSLS L^2 minimization problem

$$\mathbf{u} = \arg\min_{\mathbf{v}\in\boldsymbol{\mathcal{W}}} \mathcal{G}(\mathbf{v};\mathbf{f}) \tag{5.12}$$

and its variational form: Find $\mathbf{u}\in\boldsymbol{\mathcal{W}}$ such that

$$\mathcal{F}(\mathbf{u},\mathbf{v}) = \ell(\mathbf{v}), \tag{5.13}$$

for all $\mathbf{v}\in\boldsymbol{\mathcal{W}}$, with

$$\begin{aligned}\mathcal{F}(\mathbf{u},\mathbf{v}) &= \langle\mathcal{L}\mathbf{u},\mathcal{L}\mathbf{v}\rangle_{0,\Omega}\,,\\ \ell(\mathbf{v}) &= \langle\mathbf{f},\mathcal{L}\mathbf{v}\rangle_{0,\Omega}\,.\end{aligned}$$

We assume that bilinear functional $\mathcal{F}$ is $\boldsymbol{\mathcal{W}}$-elliptic with respect to a norm $\|\cdot\|_{\boldsymbol{\mathcal{W}}}$ in the sense that respective continuity and coercivity constants C_{cont} and C_{coer} exist, for which

$$\begin{aligned}\mathcal{F}(\mathbf{u},\mathbf{v}) &\le C_{cont}\,\|\mathbf{u}\|_{\boldsymbol{\mathcal{W}}}\,\|\mathbf{v}\|_{\boldsymbol{\mathcal{W}}}\,,\\ C_{coer}\,\|\mathbf{u}\|_{\boldsymbol{\mathcal{W}}}^2 &\le \mathcal{F}(\mathbf{u},\mathbf{u}),\end{aligned}$$

for all $\mathbf{u},\mathbf{v}\in\boldsymbol{\mathcal{W}}$.

Let $\{\Omega_j\}_{j=1,\dots,J}$ be an open partitioning of Ω such that all Ω_j are mutually disjoint and $\bigcup_{j=1}^J\overline{\Omega}_j=\overline{\Omega}$. Let $\boldsymbol{\mathcal{W}}^h$ be a finite element space for which the restriction of the operator $\mathcal{L}$ to the subdomain Ω_j is well defined. Define approximate bilinear form $\mathcal{F}^{nc}$ by

$$\mathcal{F}^{nc}(\mathbf{u}^h,\mathbf{v}^h) := \sum_{j=1}^J \left\langle\mathcal{L}\mathbf{u}^h,\mathcal{L}\mathbf{v}^h\right\rangle_{0,\Omega_j} \tag{5.14}$$

and approximate linear functional ℓ^{nc} by

$$\ell^{nc}(\mathbf{v}^h) := \sum_{j=1}^J \left\langle\mathbf{f},\mathcal{L}\mathbf{v}^h\right\rangle_{0,\Omega_j}\,, \tag{5.15}$$

for $\mathbf{u}^h,\mathbf{v}^h\in\boldsymbol{\mathcal{W}}^h$. Assume that $\mathcal{F}^{nc}$ is uniformly $\boldsymbol{\mathcal{W}}^h$-elliptic with respect to a norm $\|\cdot\|_{\boldsymbol{\mathcal{W}}^h}$, with respective continuity and coercivity constants $\tilde{C}_{cont}$ and $\tilde{C}_{coer}$. This ensures that the following approximate variational problem has a unique solution: Find $\mathbf{u}^h\in\boldsymbol{\mathcal{W}}^h$ such that

$$\mathcal{F}^{nc}(\mathbf{u}^h,\mathbf{v}^h) = \ell^{nc}(\mathbf{v}^h) \tag{5.16}$$

for all $\mathbf{v}^h \in \boldsymbol{\mathcal{W}}^h$.

THEOREM 5.2. *Consider a family of discrete problems that stem from a FOSLS L^2 minimization problem, whose associated approximate bilinear forms are uniformly $\boldsymbol{\mathcal{W}}^h$-elliptic. Then there exists a constant C, independent of the subspace $\boldsymbol{\mathcal{W}}^h$, such that*

$$\left\|\mathbf{u}-\mathbf{u}^h\right\|_{\boldsymbol{\mathcal{W}}^h} \leq C \inf_{\mathbf{v}^h \in \boldsymbol{\mathcal{W}}^h} \left\|\mathbf{u}-\mathbf{v}^h\right\|_{\boldsymbol{\mathcal{W}}^h}. \tag{5.17}$$

Proof. Let $\mathbf{v}^h \in \boldsymbol{\mathcal{W}}^h$ be arbitrary. Using $\boldsymbol{\mathcal{W}}^h$-ellipticity of $\mathcal{F}^{nc}$ and the definition of the approximate variational problem (5.16), we have

$$\begin{aligned}\tilde{C}_{coer}\left\|\mathbf{u}^h-\mathbf{v}^h\right\|^2_{\boldsymbol{\mathcal{W}}^h} &\leq \mathcal{F}^{nc}(\mathbf{u}^h-\mathbf{v}^h,\mathbf{u}^h-\mathbf{v}^h)\\ &= \mathcal{F}^{nc}(\mathbf{u}-\mathbf{v}^h,\mathbf{u}^h-\mathbf{v}^h)+\mathcal{F}^{nc}(\mathbf{u}^h-\mathbf{u},\mathbf{u}^h-\mathbf{v}^h)\\ &= \mathcal{F}^{nc}(\mathbf{u}-\mathbf{v}^h,\mathbf{u}^h-\mathbf{v}^h)+\ell^{nc}(\mathbf{u}^h-\mathbf{v}^h)-\mathcal{F}^{nc}(\mathbf{u},\mathbf{u}^h-\mathbf{v}^h).\end{aligned} \tag{5.18}$$

Using (5.14), (5.15), and the Cauchy–Schwarz inequality for any $\mathbf{w}^h \in \boldsymbol{\mathcal{W}}^h$, we have

$$\left|\ell^{nc}(\mathbf{w}^h)-\mathcal{F}^{nc}(\mathbf{u},\mathbf{w}^h)\right| \leq \sum_{j=1}^{J}\left|\left\langle \mathbf{f}-\mathcal{L}\mathbf{u},\mathcal{L}\mathbf{w}^h\right\rangle_{0,\Omega_j}\right| \leq \sum_{j=1}^{J}\left\|\mathbf{f}-\mathcal{L}\mathbf{u}\right\|_{0,\Omega_j}\left\|\mathcal{L}\mathbf{w}^h\right\|_{0,\Omega_j}.$$

Since $\mathbf{u} \in \boldsymbol{\mathcal{W}}$ is the solution of minimization problem (5.12), we deduce

$$\left\|\mathcal{L}\mathbf{u}-\mathbf{f}\right\|^2_{0,\Omega_j} \leq \mathcal{G}(\mathbf{u};\mathbf{f}) = 0$$

for all $j = 1,\ldots,J$, which implies

$$\ell^{nc}(\mathbf{w}^h)-\mathcal{F}^{nc}(\mathbf{u},\mathbf{w}^h) = 0. \tag{5.19}$$

Choosing $\mathbf{w}^h = \mathbf{u}^h - \mathbf{v}^h$ in (5.18) and appealing to the continuity of $\mathcal{F}^{nc}$, we thus have

$$\tilde{C}_{coer}\left\|\mathbf{u}^h-\mathbf{v}^h\right\|_{\boldsymbol{\mathcal{W}}^h} \leq \tilde{C}_{cont}\left\|\mathbf{u}-\mathbf{v}^h\right\|_{\boldsymbol{\mathcal{W}}^h}. \tag{5.20}$$

The triangle inequality and (5.20) imply

$$\left\|\mathbf{u}-\mathbf{u}^h\right\|_{\boldsymbol{\mathcal{W}}^h} \leq \left(\frac{C_{cont}}{C_{coer}}+1\right)\left\|\mathbf{u}-\mathbf{v}^h\right\|_{\boldsymbol{\mathcal{W}}^h},$$

which completes the proof. ∎

Remark 3. Uniform $\boldsymbol{\mathcal{W}}^h$ coercivity must be established before Theorem 5.2 can be applied.

Theorem 5.2 implies that, for a FOSLS L^2 formulation that is discretized using a nonconforming finite element space, an estimate analogous to Cea's lemma (cf. [16, Theorem 13.1]) holds. Inequality (5.17) does not involve a consistency error term, as in the fundamental estimate for nonconforming finite elements (see [1], commonly referred to as Strang's second lemma). In common use is a patch test (cf. [16, p. 221]), which determines whether this consistency error term approaches zero as $h \to 0$. The corollary shows that, in the FOSLS L^2 context, elements that do not satisfy such conditions can be used, provided that uniform $\boldsymbol{\mathcal{W}}^h$-ellipticity can be established for $\mathcal{F}^{nc}$ and an error estimate based solely on interpolation theory can be derived.

5.3. An error estimate in the nonconforming space $\mathbf{W}^h \not\subseteq \mathbf{W}$. The finite element space $\mathbf{W}^h$ contains singular functions that would ideally model the singular behavior of the solution at cross-points exactly. However, the exponents and coefficients of these singular functions can be calculated only approximately, which means generally that $\mathbf{W}^h \not\subseteq \mathbf{W}$.

We will use Theorem 5.2 to derive an error estimate for the nonconforming case. However, as noted in Remark 3, we first must establish uniform coercivity of the approximate bilinear form. Define the nonconforming functional by

$$G^{nc}(\mathbf{u}; f) = \sum_{i=1}^{J} \left\| \frac{1}{\sqrt{a}} (\nabla \cdot \sqrt{a}\mathbf{u} + f) \right\|_{0,\Omega_i}^2 + \left\| \frac{1}{\sqrt{a}} \nabla \times \left(\frac{\mathbf{u}}{\sqrt{a}} \right) \right\|_{0,\Omega_i}^2, \tag{5.21}$$

the associated bilinear form

$$\mathcal{F}^{nc}(\mathbf{u}, \mathbf{v}) = \sum_{i=1}^{K} \left\langle \frac{1}{\sqrt{a}} \nabla \cdot \sqrt{a}\mathbf{u}, \frac{1}{\sqrt{a}} \nabla \cdot \sqrt{a}\mathbf{v} \right\rangle_{\Omega_i}^2 + \left\langle \sqrt{a} \nabla \times \frac{1}{\sqrt{a}\mathbf{u}}, \sqrt{a} \nabla \times \frac{1}{\sqrt{a}} \mathbf{v} \right\rangle_{\Omega_i}^2, \tag{5.22}$$

and the seminorm

$$\mathcal{F}^{nc}(\mathbf{u}, \mathbf{u}) := |\mathbf{u}|_{\mathbf{W}^h}^2. \tag{5.23}$$

We show in Appendix A.2 that $\mathcal{F}^{nc}$ is uniformly coercive in the norm $\|\mathbf{u}\|_{\mathbf{W}^h}^2 := \|\mathbf{u}\|_0^2 + |\mathbf{u}|_{\mathbf{W}^h}^2$. Thus, in what follows we use the seminorm. Now Theorem 5.2 implies that

$$\mathcal{F}^{nc}(\mathbf{u} - \mathbf{u}^h, \mathbf{u} - \mathbf{u}^h)^{1/2} = \left| \mathbf{u} - \mathbf{u}^h \right|_{\mathbf{W}^h} \leq C \inf_{\mathbf{v}^h \in \mathbf{W}^h} \left| \mathbf{u} - \mathbf{v}^h \right|_{\mathbf{W}^h}. \tag{5.24}$$

Denote by $\delta_m^h \tilde{\mathbf{s}}_{m,n}$ an approximation of the singular basis function $\delta_m^h \mathbf{s}_{m,n}$ such that $\tilde{\mathbf{s}}_{m,n}$ can be written in the general form (3.5) with approximate exponent $\tilde{\alpha}_{m,n}$ and approximate coefficient vectors $\tilde{\lambda}_{m,n}$ and $\tilde{\mu}_{m,n}$. The exact solution $\mathbf{u} \in \mathbf{W}$ of the FOSLS minimization problem (2.4) has the form

$$\mathbf{u} = \mathbf{u}_0 + \sum_{m=1}^{M} \sum_{n=1}^{N_m} \omega_{m,n} \delta_m^h \mathbf{s}_{m,n} + \sum_{m=1}^{M} \sum_{n=1}^{N_m} \omega_{m,n} \left(\delta_m^H - \delta_m^h \right) \mathbf{s}_{m,n}, \tag{5.25}$$

with $\mathbf{u}_0 \in \mathbf{W}_S^1$ independent of h. We choose

$$\mathbf{v}^h := I^h \mathbf{u}_0 + \sum_{m=1}^{M} \sum_{n=1}^{N_m} \omega_{m,n} \delta_m^h \tilde{\mathbf{s}}_{m,n} + \sum_{m=1}^{M} \sum_{n=1}^{N_m} \omega_{m,n} \left(\delta_M^H - \delta_m^h \right) \tilde{\mathbf{s}}_{m,n},$$

where I^h is the interpolant operator that was introduced in (5.5). Using (5.24) and the triangle inequality, we have

$$\begin{aligned} \left| \mathbf{u} - \mathbf{u}^h \right|_{\mathbf{W}^h, \Omega_j} \leq C \left| \mathbf{u}_0 - \mathbf{v}^h \right|_{\mathbf{W}^h, \Omega_j} &+ \sum_{m=1}^{M} \sum_{n=1}^{N_m} |\omega_{m,n}| \left| \delta_m^h \left(\mathbf{s}_{m,n} - \tilde{\mathbf{s}}_{m,n} \right) \right|_{\mathbf{W}^h, \Omega_j} \\ &+ \sum_{m=1}^{M} \sum_{n=1}^{N_m} |\omega_{m,n}| \left| \left(\delta_m^H - \delta_m^h \right) \left(\mathbf{s}_{m,n} - \tilde{\mathbf{s}}_{m,n} \right) \right|_{\mathbf{W}^h, \Omega_j}, \end{aligned} \tag{5.26}$$

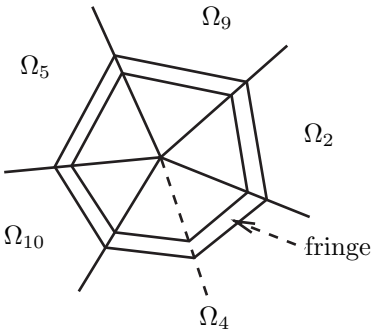

FIG. 5.2. *Geometry of interfaces meeting at a cross-point. Here,* $I_m = 5$, $\{j_i\} = \{2, 9, 5, 10, 4\}$.

for $j = 1, \ldots, J$. Standard interpolation error estimates can be used to estimate $|\mathbf{u}_0 - I^h\mathbf{u}_0|_{\mathbf{W}^h,\Omega_j}$, analogously to the proof of Theorem 5.1. We now derive estimates for the remaining terms, which involve the singular basis functions and their approximations.

Let $\Omega_{j_i} \subset \Omega$, $i = 1, \ldots, I_m$, be the set of subdomains that meet at cross-point m, ordered so that they appear consecutively with increasing i. (See Figure 5.2.) Let $\{\vartheta_{j_i}\}_{i=1,\ldots,I_m}$ be the set of angles at cross-point m. If the difference of two subsequent angles is greater than $\pi/2$, then we introduce artificial interfaces, equally spaced in the interval $(\vartheta_{j_i}, \vartheta_{j_{i+1}})$, such that the angles between subsequent interfaces are now smaller than $\pi/2$. (See the dashed interface line in Figure 5.2.) The platform and fringe are such that, for subdomains that do not require an artificial interface, $\Omega_{j_i} \cap (P_m \cup F_m)$ is an isosceles triangle. In the presence of artificial interfaces, platform and fringe are such that their intersection with Ω_{j_i} is the union of isosceles triangles whose sides are aligned with the artificial interfaces.

In the following calculations, we denote by $\tilde{I}_m$ the total number of actual and artificial interfaces, and by $\{\theta_{m,i}\}_{i=1,\ldots,\tilde{I}_m}$ the angles of these interfaces, ordered such that $\theta_{m,i} < \theta_{m,i+1}$, $i = 1, \ldots, \tilde{I}_m$ (define $\theta_{m,\tilde{I}_m+1} = 2\pi + \theta_{m,1}$). $P_{m,i}$ and $F_{m,i}$ are the parts of platform and fringe, respectively, that are enclosed by angles $\theta_{m,i}$ and $\theta_{m,i+1}$, $i = 1, \ldots, \tilde{I}_m$. Denote by $R_{m,i}$ the distance from $F_{m,i}$ to the cross-point, and by $h_{m,i}$ the radial width of $F_{m,i}$. We omit the subscript $_{m,n}$ for singular functions, when it is obvious to which singular functions we refer.

The cut-off function on $F_{m,i}$, for $\theta \in (\theta_{m,i}, \theta_{m,i+1})$, is

$$\delta^h(r,\theta) = \frac{\cos\left(\theta_{m,i+1/2} - \theta\right)}{h}\left(\frac{R_{m,i} + h_{m,i}}{\cos\left(\theta_{m,i+1/2} - \theta\right)} - r\right), \tag{5.27}$$

where $\theta_{m,i+1/2} = (\theta_{m,i+1} - \theta_{m,i})/2$, with partial derivatives

$$\delta^h_x(r,\theta) = -\frac{\cos\theta_{m,i+1/2}}{h}, \qquad \delta^h_y(r,\theta) = -\frac{\sin\theta_{m,i+1/2}}{h}. \tag{5.28}$$

In what follows, we assume the approximate singular basis functions, $\tilde{\mathbf{s}}_{m,n}$, are of the form (3.5), with known but inexact coefficients $\tilde{\alpha}_{m,n} = \alpha_{m,n} + \eta_m$, $\tilde{\lambda}_{m,n} = \lambda_{m,n} + O(\eta_m)$, and $\tilde{\mu}_{m,n} = \mu_{m,n} + O(\eta_m)$. We will drop subscripts where the meaning is clear.

LEMMA 5.3. *Let* $\eta_{m,n} = |\alpha_{m,n} - \tilde{\alpha}_{m,n}|$. *The estimate*

$$\left|\delta^h_m \mathbf{s}_{m,n} - \delta^h_m \tilde{\mathbf{s}}_{m,n}\right|^2_{\mathbf{W}^h} \leq \frac{C(a)\eta^2_{m,n}}{h} \tag{5.29}$$

holds for all cross-points and singular basis functions and some constant $C(a)$ independent of h and η.

Proof. Omitting the subscripts $_{m,n}$ for convenience, note that

$$\mathcal{F}^{nc}_{P_m}(\delta^h_m \mathbf{s}, \delta^h_m \mathbf{s}) = \mathcal{F}^{nc}_{P_m}(\delta^h_m \tilde{\mathbf{s}}, \delta^h_m \mathbf{s}) = \mathcal{F}^{nc}_{P_m}(\delta^h_m \tilde{\mathbf{s}}, \delta^h_m \tilde{\mathbf{s}}) = 0,$$

where P_m is the platform associated with singular function $\mathbf{s}$. Letting $\mathbf{s} = (s_1, s_2)^t$ and $\tilde{\mathbf{s}} = (\tilde{s}_1, \tilde{s}_2)^t$, (5.28) and some vector calculus implies

$$\begin{aligned}
\left|\delta^h \mathbf{s} - \delta^h \tilde{\mathbf{s}}\right|^2_{\mathbf{W}^h, F_{m,i}} &= \left\|\nabla \cdot \left(\delta^h \mathbf{s} - \delta^h \tilde{\mathbf{s}}\right)\right\|^2_{0,F_{m,i}} + \left\|\nabla \times \left(\delta^h \mathbf{s} - \delta^h \tilde{\mathbf{s}}\right)\right\|^2_{0,F_{m,i}} \\
&= \left\|\nabla \delta^h \cdot (\mathbf{s} - \tilde{\mathbf{s}})\right\|^2_{0,F_{m,i}} + \left\|\nabla^\perp \delta^h \cdot (\mathbf{s} - \tilde{\mathbf{s}})\right\|^2_{0,F_{m,i}} \\
&= \frac{1}{h^2_{m,i}} \left(\|s_1 - \tilde{s}_1\|^2_{0,F_{m,i}} + \|s_2 - \tilde{s}_2\|^2_{0,F_{m,i}} \right). \qquad (5.30)
\end{aligned}$$

We now estimate only the last term in (5.30), since a similar estimate can be derived analogously for the other term. Let $\eta_\lambda = \lambda - \tilde{\lambda}$ and $\eta_\mu = \mu - \tilde{\mu}$, and note that η_λ and η_μ are of order $O(\eta)$. Then we get

$$\begin{aligned}
\|s_2 - \tilde{s}_2\|^2_{0,F_{m,i}} &= a_i \left\| \alpha r^{\alpha-1} (\lambda \cos(\alpha - 1)\theta - \mu \sin(\alpha - 1)\theta) \right. \\
&\qquad \left. -\tilde{\alpha} r^{\tilde{\alpha}-1} (\tilde{\lambda} \cos(\alpha_h - 1)\theta - \tilde{\mu} \sin(\tilde{\alpha} - 1)\theta) \right\|^2_{0,F_{m,i}} \\
&= a_i \left\| (\alpha r^{\alpha-1} - \tilde{\alpha} r^{\tilde{\alpha}-1})(\lambda \cos(\alpha - 1)\theta - \mu \sin(\alpha - 1)\theta) \right. \\
&\qquad \left. -\tilde{\alpha} r^{\tilde{\alpha}-1} (\eta_\lambda \cos(\tilde{\alpha} - 1)\theta - \eta_\mu \sin(\tilde{\alpha} - 1)\theta) \right\|^2_{0,F_{m,i}} \qquad (5.31) \\
&\le 2a_i \left\| (\alpha r^{\alpha-1} - \tilde{\alpha} r^{\tilde{\alpha}-1})(\lambda \cos(\alpha - 1)\theta - \mu \sin(\alpha - 1)\theta) \right\|^2_{0,F_{m,i}} \\
&\quad + 2a_i \left\| \tilde{\alpha} r^{\tilde{\alpha}-1} (\eta_\lambda \cos(\tilde{\alpha} - 1)\theta - \eta_\mu \sin(\tilde{\alpha} - 1)\theta) \right\|^2_{F_{m,i}} \\
&\le 4a_i(\lambda^2 + \mu^2) \left\| \alpha r^{\alpha-1} - \tilde{\alpha} r^{\tilde{\alpha}-1} \right\|^2_{F_{m,i}} + 4a_i(\eta^2_\lambda + \eta^2_\mu) \left\| \tilde{\alpha} r^{\tilde{\alpha}-1} \right\|^2_{F_{m,i}}.
\end{aligned}$$

Let $0 < r < R + h$, $0 < h < 1$, and $0 < \eta < 1$. Then we have

$$|1 - r^\eta| \le C_1 \eta, \qquad \left\| \tilde{\alpha} r^{\tilde{\alpha}-1} \right\|^2_{0,F_{m,i}} \le C_2 h_{m,i}, \qquad (5.32)$$

which, with $0 < \alpha, \tilde{\alpha} \le 1$, implies that

$$\begin{aligned}
\left\| \alpha r^{\alpha-1} - \tilde{\alpha} r^{\tilde{\alpha}-1} \right\|^2_{0,F_{m,i}} &\le \left\| \alpha (r^{\alpha-1} - r^{\tilde{\alpha}-1}) - \eta r^{\tilde{\alpha}-1} \right\|^2_{0,F_{m,i}} \\
&\le 2 \left\| r^{\alpha-1} - r^{\tilde{\alpha}-1} \right\|^2_{0,F_{m,i}} + 2\eta^2 \left\| r^{\tilde{\alpha}-1} \right\|^2_{0,F_{m,i}} \\
&\le 2 \left\| r^{\alpha-1} (1 - r^\eta) \right\|^2_{0,F_{m,i}} + 2\eta^2 C_2 h_{m,i} \qquad (5.33) \\
&\le 2C_1^2 \eta^2 C_2 h_{m,i} + 2\eta^2 C_2 h_{m,i} \\
&= C\eta^2 h_{m,i}.
\end{aligned}$$

Combining estimates (5.31)–(5.33) with (5.30), we get

$$\left|\delta^h \mathbf{s} - \delta^h \tilde{\mathbf{s}}\right|_{\mathbf{W}^h, F_{m,i}} \le \frac{C(a_i)\eta^2}{h_{m,i}}. \qquad (5.34)$$

TABLE 5.1
Diameter of the fringe is fixed $= 1/6$ *on all levels,* $\Omega = (0,1)^2$.

	With quadratics		Without quadratics	
h	$\mathcal{G}(\mathbf{u}^h; f)$	ratio	$\mathcal{G}(\mathbf{u}^h; f)$	ratio
1/24	4.29(-2)	1.81	9.66(-2)	1.11
1/48	2.37(-2)	2.49	8.68(-2)	1.20
1/96	9.51(-3)	3.14	7.22(-2)	1.34
1/192	3.02(-3)	3.56	5.36(-2)	1.52
1/384	8.48(-4)	3.78	3.52(-2)	1.69
1/768	2.24(-4)		2.08(-2)	

Summing over interfaces and artificial interfaces, and noting that $h_{m,i} = O(h)$, completes the proof. □

Using estimates (5.7) and (5.29) in (5.26) implies the main result of this section.

THEOREM 5.4. *Denote by* $\mathbf{u} \in \mathbf{W}$ *the solution of minimization problem* (2.4) *and by* $\mathbf{u}^h \in \mathbf{W}^h$ *the solution of the discretized variational problem* (2.7). *Also, let* $\eta > 0$ *be the maximum error in the exponent of the approximate singular basis function,* h *be the mesh size of triangulation* $\mathcal{T}^h$ *and the fringe width, and*

(5.35)
$$\kappa := \min_{\mathbf{s}}\{\alpha : \alpha \text{ is the exponent of } \mathbf{s}, \alpha > 1, \nabla \cdot (\sqrt{a}\mathbf{s}) = 0, \text{ and } \nabla \times (\mathbf{s}/\sqrt{a}) = 0\}.$$

Then

$$\left|\mathbf{u} - \mathbf{u}^h\right|_{\mathbf{W}^h} \leq C(a)\left(h^{\kappa-1} + \eta/\sqrt{h}\right), \tag{5.36}$$

where the constant $C(a)$ *does not depend on* η, κ, *and* h.

To achieve a discretization error of order $O(h)$ in the nonconforming finite element space $\mathbf{W}^h$, we must ensure that $\kappa \geq 2$ and that the approximation error in the exponent η is of order $O(h^{3/2})$. The constraint on κ can be met by adding basis functions of the general form (3.5) that have exponents $1 < \alpha < 2$ and satisfy the first two equations in (2.2) with $f = 0$.

5.4. An example. Here, we present a numerical example to illustrate the theoretical results of the previous sections. We consider problem (2.2) on the unit square, with $f = 0$ and the Dirichlet boundary condition

$$\tau \cdot \mathbf{u} = \tau \cdot \mathbf{s} \quad \text{on } \partial(0,1)^2, \tag{5.37}$$

where $\mathbf{s}$ is the singular function associated with the coefficient

$$a(x,y) = \begin{cases} 1 & \text{for } 0 < x, y < 1/2 \text{ and } 1/2 < x, y < 1, \\ 100 & \text{elsewhere in } (0,1)^2. \end{cases} \tag{5.38}$$

For this checkerboard pattern, the exponent is approximately $\alpha \approx 0.126902069$.

Table 5.1 shows the value of the FOSLS functional at the solution for various values of h. The left two columns show results for the finite element space $\mathbf{W}^h$ consisting of linear, quadratic, and singular elements as described in section 4. The right two columns show results for a finite element space that contains only the linear and singular elements. The ratio refers to the quotient of two subsequent functional values: ratio $= \mathcal{G}(\mathbf{u}^h; f)/\mathcal{G}(\mathbf{u}^{h/2}; f)$. For the space $\mathbf{W}^h$, this ratio approaches 4 as h is decreased. In the space that does not contain quadratic elements in the fringe, the ratio approaches 2 for decreasing h. These results signal a lower approximation order when quadratic elements are not included in the finite element space.

6. A multilevel solver. We now describe a multilevel solver for the linear system that arises from the finite element discretization using $\mathbf{W}^h$. Our goal is to use standard coarsening for linear elements and to include singular basis functions on every level. This results in a hierarchy of spaces $\mathbf{W}^{2^K h} \not\subseteq \mathbf{W}^{2^{K-1} h} \not\subseteq \cdots \not\subseteq \mathbf{W}^{2h} \not\subseteq \mathbf{W}^h$. The spaces are nested except for the singular basis functions, which are nonnested, since the fringes on different levels have different widths.

We coarsen such that the platform associated with a given cross-point has equal size on all levels. The choice of interpolation and restriction for linear and quadratic elements in fringes is driven by the interpolation for singular basis functions.

Consider interpolation of $\delta_m^{2h}\tilde{\mathbf{s}}_{m,n} \in \mathbf{W}^{2h}$ to $\mathbf{W}^h$. The coefficient $\omega_{m,n}^{2h}$ of $\delta_m^{2h}\tilde{\mathbf{s}}_{m,n}$ is transferred by injection: $\omega_{m,n}^h \leftarrow \omega_{m,n}^{2h}$. What is left is the difference $(\delta_m^{2h} - \delta_m^h)\tilde{\mathbf{s}}_{m,n}$ that is interpolated using standard linear and quadratic interpolation. Denote by N_L^h and N_Q^h the respective numbers of linear and quadratic basis functions in $\mathbf{W}^h$, and by $\boldsymbol{\psi}_l$, $l = 1, \ldots, N_L^h$, and $\boldsymbol{\phi}_k$, $k = 1, \ldots, N_Q^h$, the respective linear and quadratic basis functions in $\mathbf{W}^h$, such that

$$\begin{aligned}(6.1)\quad \mathbf{W}^h = \operatorname{span}\left\{\boldsymbol{\psi}_l \;:\; l = 1, \ldots, N_L^h\right\} \;\cup\; \operatorname{span}\left\{\boldsymbol{\phi}_k \;:\; k = 1, \ldots, N_Q^h\right\} \\ \cup\; \operatorname{span}\left\{\delta_m^h \tilde{\mathbf{s}}_{m,n} \;:\; m = 1, \ldots, M;\; n = 1, \ldots, N_m\right\}.\end{aligned}$$

Define the vectors $\boldsymbol{\beta}_{m,n}^h = \{\beta_{m,n}^{h,l}\}_{l=1,\ldots,N_L^h}$ and $\boldsymbol{\gamma}_{m,n}^h = \{\gamma_{m,n}^{h,k}\}_{k=1,\ldots,N_Q^h}$ so that their elements are the respective coefficients of linear and quadratic basis functions of the pointwise linear and quadratic interpolant of $(\delta_m^{2h} - \delta_m^h)\tilde{\mathbf{s}}_{m,n}$. We now have

$$(6.2)\qquad I^h(\delta_m^{2h} - \delta_m^h)\tilde{\mathbf{s}}_{m,n} := \sum_{l=1}^{N_L^h} \beta_l^h \boldsymbol{\psi}_{m,n}^{h,l} + \sum_{k=1}^{N_Q^h} \gamma_k^h \boldsymbol{\phi}_{m,n}^{h,k}.$$

Note that most of the $\beta_{m,n}^{h,l}$ and $\gamma_{m,n}^{h,k}$ are zero, since $\delta_m^{2h} - \delta_m^h$ is nonzero only in the fringe of level $2h$ associated with cross-point m.

Assume that the basis functions are ordered so that the first N_L^h are linear, the next N_Q^h are quadratic, and the last $N_S := \sum_{m=1}^M N_m$ are singular basis functions. Then the column in interpolation matrix $\mathcal{I}_{2h}^h$ corresponding to the singular basis function with index (m, n) is $(\beta_{m,n}^{h,1}, \ldots, \beta_{m,n}^{h,N_L^h}, \gamma_{m,n}^{h,1}, \ldots, \gamma_{m,n}^{h,N_Q^h}, 0, \ldots, 0, 1, 0, \ldots, 0)$. Fine-level linear basis functions centered at vertices inside the coarse-level fringe are interpolated using standard linear interpolation.

Figure 6.1 shows a section of the fringe in a triangular mesh of mesh size h (thick and thin lines), and a section of the fringe in the coarsened triangular mesh of mesh size $2h$ (thick lines). It illustrates the location of the quadratic nodes on both levels.

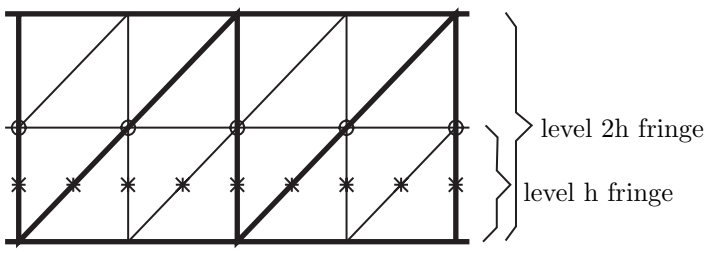

FIG. 6.1. *Location of quadratic points (level h: stars; level 2h: circles).*

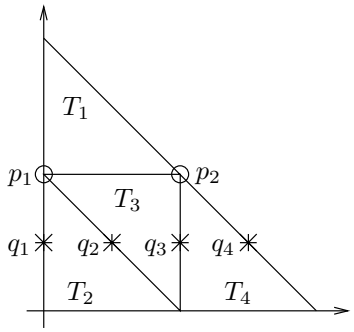

FIG. 6.2. *Coarse fringe triangle subdivided into four subtriangles.*

Note that quadratic nodes on level $2h$ coincide with vertices of triangles on level h. We now describe the interpolation formulas that are used for quadratic nodes on level h and linear nodes on level h that coincide with quadratic nodes on level $2h$. For the latter, we use linear interpolation from the two neighboring coarse points and add to that the value of the quadratic at that point.

Figure 6.2 shows a coarse fringe unit triangle in general (ξ, η) coordinates that is subdivided into four subtriangles $T_1, \ldots, T_4$. Triangles T_2, T_3, T_4 are in the fine fringe. Coarse-level quadratic basis functions are centered at points q_1^c and q_2^c, and fine-level quadratic basis functions are centered at points $q_1^f, \ldots, q_4^f$. (We denote by $q_1^c, q_2^c, q_1^f, \ldots, q_4^f$ the respective points, as well as the coefficients of quadratic basis functions at these points.) Assume that the linear part of the coarse-level function is zero. The quadratic part is

$$Q(\xi, \eta) = q_1^c Q_1^c(\xi, \eta) + q_2^c Q_2^c(\xi, \eta),$$

with

$$\begin{aligned} Q_1^c(\xi, \eta) &= 4\eta(1 - \xi - \eta), \\ Q_2^c(\xi, \eta) &= 4\xi\eta. \end{aligned}$$

First we interpolate the linear fine-level points that coincide with quadratic coarse-level points. We obtain the following linear functions:

$$\begin{aligned} L_2(\xi, \eta) &= 2\eta q_1^c && \text{in } T_2, \\ L_3(\xi, \eta) &= 2\eta(2(q_1^c - q_2^c)\xi - q_1^c) && \text{in } T_3, \\ L_4(\xi, \eta) &= 2\eta q_2^c && \text{in } T_4. \end{aligned}$$

We want the interpolant to be pointwise exact at fine-level quadratic points, so interpolation of fine-level quadratic points is determined by

$$\begin{array}{rcccl} q_1^f & = & Q(0, 1/4) - L_2(0, 1/4) & = & 1/4\ q_1^c, \\ q_2^f & = & Q(1/4, 1/4) - L_2(1/4, 1/4) & = & 1/4\ q_2^c, \\ q_3^f & = & Q(1/2, 1/4) - L_4(1/2, 1/4) & = & 1/4\ q_1^c, \\ q_4^f & = & Q(3/4, 1/4) - L_4(3/4, 1/4) & = & 1/4\ q_2^c. \end{array} \tag{6.3}$$

Interpolation weights in (6.3) do not depend on ξ or η, so they are the same in (x, y) coordinates.

Denote by $\hat{I}_{2h}^h \in \Re^{(N_L+N_Q)\times(N_L+N_Q)}$ the matrix that interpolates linear and quadratic basis functions on level h from level $2h$, as defined above. Let $B^h := \{\boldsymbol{\beta}_{m,n}^h\}_{n=1,\ldots,N_m;m=1,\ldots,M}$ and $\Gamma^h := \{\boldsymbol{\gamma}_{m,n}^h\}_{n=1,\ldots,N_m;m=1,\ldots,M}$. Then we can write the interpolant operator $\mathcal{I}_{2h}^h : \mathbf{W}^{2h} \to \mathbf{W}^h$ in matrix form as

$$\mathcal{I}_{2h}^h = \begin{pmatrix} & \hat{I}_{2h}^h & & B^h \\ & & & \Gamma^h \\ 0 & 0 & & I \end{pmatrix}, \tag{6.4}$$

where I is the identity matrix in $\Re^{N_S\times N_S}$.

We extend this idea to all levels to obtain interpolation matrices $\mathcal{I}_{2^K h}^{2^{K-1}h}, \ldots, \mathcal{I}_{2h}^h$. The restriction operators are defined as the transpose of interpolation $\mathcal{I}_{2^k h}^{2^{k+1}h} = (\mathcal{I}_{2^{k+1}h}^{2^k h})^t$ for $k = 0, \ldots, K-1$. The coarse-grid stiffness matrix is determined from the Galerkin principle by fine-grid stiffness matrix S^h and interpolation matrix $\mathcal{I}_{2h}^h$:

$$S^{2h} = (\mathcal{I}_{2h}^h)^t \; S^h \; \mathcal{I}_{2h}^h. \tag{6.5}$$

This definition is extended recursively to all levels.

We use Gauss–Seidel relaxation for pre- and postrelaxation in the multigrid iteration and solve the coarse grid problem approximately using algebraic multigrid (AMG) (see [29]). Numerical tests have shown that the standard AMG algorithm is not well suited to solving the resulting linear system. Therefore, we instead use a Schur complement approach that exploits the structure of the coarse-grid problem, with the subproblems treated by AMG.

To explain this Schur-AMG approach, note that the coarse-grid linear system has the general form

$$\begin{pmatrix} A & V \\ V^t & D \end{pmatrix} \begin{pmatrix} \mathbf{u} \\ \mathbf{w} \end{pmatrix} = \begin{pmatrix} \mathbf{f} \\ \mathbf{g} \end{pmatrix}, \tag{6.6}$$

where submatrix A represents connections between linear and quadratic basis functions and D represents connections between singular basis functions. A is sparse and D is block diagonal. The off-diagonal submatrix V represents connections between the linear and quadratic basis functions and the singular basis functions. Linear system (6.6) can be reduced to

$$\mathbf{u} = A^{-1}\mathbf{f} - A^{-1}V\mathbf{w}, \tag{6.7}$$

$$\mathbf{w} = (D - V^t A^{-1} V)^{-1}(\mathbf{g} - V^t A^{-1}\mathbf{f}). \tag{6.8}$$

We calculate $A^{-1}\mathbf{f}$ and $A^{-1}V$ approximately using AMG. The inverse of $D - V^t A^{-1} V$ is then calculated directly, using Gaussian elimination, since the number of singular basis functions is assumed to be small.

Denote by N_C the number of coarse-grid linear and quadratic basis functions and by N_S the number of singular basis functions. Thus, $A \in \Re^{N_C\times N_C}$, $V \in \Re^{N_C\times N_S}$, and $D \in \Re^{N_S\times N_S}$. AMG has complexity of order $O(N_C)$, and the inverse of $D - V^t A^{-1} V$ can be calculated in $O(N_S^3)$ operations. Hence, the complexity of the coarse-grid solver is of order $O(N_S^3 + N_S N_C)$. Since N_S is assumed to be small in comparison to N_C, we can deduce that standard multilevel complexity analysis applies (see, for example, [31]).

TABLE 7.1
Influence of the coefficient $a(x,y)$ ($W(2,2)$ cycle).

	$a(x,y) \in \{1,100\}$				$a(x,y) \in \{1,10000\}$			
Levels =	3	4	5	6	3	4	5	6
1×1	.20	.15	.13	.13	.27	.23	.13	.13
2×2	.28	.23	.13	.13	.37	.35	.24	.13
3×3	.33	.29	.18	.13	.40	.42	.32	.17
4×4	.38	.36	.25	.13	.45	.48	.39	.23

TABLE 7.2
Effective convergence factors: influence of the number of relaxations ($a(x,y) \in [1,100]$).

	$W(1,1)$				$W(2,2)$				$W(4,4)$			
Levels =	3	4	5	6	3	4	5	6	3	4	5	6
1×1	.30	.24	.27	.27	.45	.39	.36	.36	.64	.59	.49	.49
2×2	.39	.34	.26	.26	.53	.48	.36	.36	.71	.68	.58	.49
3×3	.44	.36	.30	.26	.57	.54	.42	.36	.74	.72	.63	.49
4×4	.48	.47	.37	.26	.62	.60	.50	.36	.75	.72	.63	.49

7. Numerical results. To study the convergence properties of the multigrid algorithm described above let the domain Ω be a square partitioned in a checkerboard fashion into square subdomains of equal size, where the coefficient a is constant. In our examples, a takes on two values that are distributed over the square subdomains in a checkerboard fashion. We report asymptotic convergence factors of the functional value $(\mathcal{G}(\mathbf{u}^h; f))^{1/2}$ that were obtained by setting $f = 0$ and imposing homogeneous Dirichlet boundary conditions $\mathbf{n} \times \sqrt{a}\mathbf{u}^h = 0$ on $\partial\Omega$. Thus, the exact solution of the problem is $\mathbf{u}^h = 0$, which allows us to perform many iterations without encountering serious machine representation effects. To properly test convergence, we initialize all variables randomly.

Table 7.1 shows asymptotic convergence factors for the $W(2,2)$ cycle for two examples of a. Four checkerboard patterns are investigated, ranging from one singular basis function to 16. Each column shows asymptotic convergence factors for fixed mesh-size h. Hence, the domain Ω changes for varying numbers of singular basis functions. However, the width of fringes does not change.

We observe that, for a larger number of levels, typical multigrid convergence factors that are h-independent are attained. For a smaller number of levels, the convergence factors appear to grow with the number of singular basis functions. However, this dependency appears to weaken as more levels are added; it appears to be stronger for larger jumps in the coefficient a.

In Table 7.2, the influence of the number of pre- and postrelaxation steps in the W-cycle is shown. We display effective convergence factors relative to the $W(1,1)$ cycle. Since for integer $k > 1$ one $W(k,k)$ cycle is k times more costly than one $W(1,1)$ cycle, we have $\rho_{W(k,k),\text{effective}} = \rho_{W(k,k)}^{1/k}$. Increasing the number of pre- and postrelaxation steps increases effective convergence factors. It is, hence, most efficient to use $W(1,1)$ cycles.

Table 7.3 shows results for two convergence tolerances for the AMG iteration that is used to invert A approximately. For the larger tolerance of $1e-1$ convergence of the multilevel iteration is somewhat slower than for the smaller tolerance of $1e-9$. This difference is less pronounced when more levels are added.

TABLE 7.3
Influence of the coarse grid solver on the overall convergence ($W(2,2)$ cycles, $a(x,y) \in \{1, 100\}$).

AMG tolerance =	$1e-9$				$1e-1$			
Geometry\levels =	3	4	5	6	3	4	5	6
1×1	.20	.15	.13	.13	.22	.15	.13	.13
2×2	.28	.23	.13	.13	.42	.31	.17	.13
3×3	.33	.29	.18	.13	.51	.40	.24	.13
4×4	.38	.36	.25	.13	.59	.51	.35	.17

8. Conclusions. We introduced a finite element method for FOSLS L^2 formulation of the diffusion equation with discontinuous coefficients. Our approach uses singular basis functions to yield accurate approximation of the flux variable close to singular points in the domain at minimal additional computational cost. Stress intensity factors are also calculated. We developed a special discretization error analysis, since standard theory is not applicable. This led to a general error estimate for FOSLS L^2 discretizations with nonconforming finite elements. We also proposed a multilevel algorithm for the solution of the resulting linear system that uses nonstandard coarse spaces including coarse representations of singular basis functions. The performance of the algorithm is illustrated by numerical examples.

Appendix A. Uniform coercivity of $\mathcal{F}^{nc}$. The purpose of this appendix is to establish the uniform coercivity of $\mathcal{F}^{nc}$. In [2] such a bound was established for the conforming functional. Here, we show that the coercivity constant will be independent of h and η, the error in the exponents of the singular basis function, only if η goes to zero at least as fast as the cosine of the angle between the mesh-dependent singular function $\delta_m^h \mathbf{s}_{m,n}^\eta$ and the subspace, $\mathbf{W}_S^1$, of piecewise H^1 functions. Unfortunately, a proof that the angle between the singular basis functions and $\mathbf{W}_S^1$ is $O(h)$ has not been found. In this next section we provide numerical proof.

A.1. Angle between $\delta_m^h \mathbf{s}_{m,n}$ and W_S^1. In the example we present in Figure A.1, the domain Ω is divided into subdomains in a 2×2 checkerboard fashion, with $a = 1$ in the upper left and lower right subdomains, and $a = 100$ in the upper right and lower left subdomains. This configuration results in a singularity in the center of the domain with exponent $\alpha \approx 0.126902$. Figure A.1 depicts $1 - \cos\theta$ as a function of h, where θ is the angle between the singular basis function and the rest of

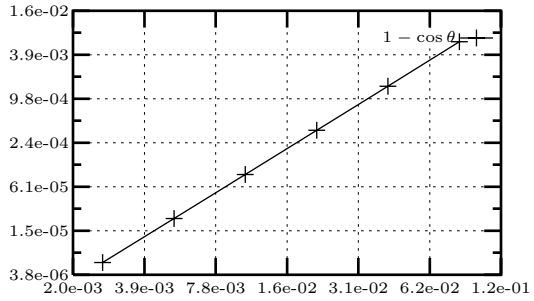

FIG. A.1. *A $\log_2$-$\log_2$ plot of $1 - \cos\theta$ (see (A.1)), where h is on the x-axis. θ is the angle between a singular basis function and the rest of the space.*

the space,

$$\cos\theta = \frac{\mathcal{F}^{nc}(\delta^h \mathbf{s}^h, I^h(\delta^h \mathbf{s}^h))}{\mathcal{F}^{nc}(\delta^h \mathbf{s}^h, \delta^h \mathbf{s}^h)^{1/2}\mathcal{F}^{nc}(I^h(\delta^h \mathbf{s}^h), I^h(\delta^h \mathbf{s}^h))^{1/2}}, \tag{A.1}$$

and I^h is the standard pointwise linear interpolation operator.

Both axes in the figure are on a $\log_2$ scale. All data points lie on a straight line, so we conjecture $1 - \cos\theta = O(h^2)$, and hence $\theta = O(h)$.

A.2. Uniform coercivity. We assume that the discrete space consists of the conforming linears and quadratics, with proper jumps across the interfaces, plus a finite number of singular basis functions. Here, as in section 5, we make the assumption that the approximate singular basis functions $\tilde{\mathbf{s}}_{m,n}$ are of the form (3.5), with known but inexact coefficients $\tilde{\alpha}_{m,n} = \alpha_{m,n} + \eta_{m,n}$, $\tilde{\lambda}_{m,n} = \lambda_{m,n} + O(\eta_{m,n})$, and $\tilde{\mu}_{m,n} = \mu_{m,n} + O(\eta_{m,n})$. We will drop subscripts where the meaning is clear.

We further assume that $\eta_{m,n}$ is sufficiently small to resolve the differences between exponents at a given singular point $\mathbf{x}_m$. That is, we assume that $\eta_{m,n} \leq \eta_{m,0}$ for $n = 1, \ldots, N_m$.

To emphasize the dependence on η, we denote the discrete subspace as

$$\mathbf{W}^{h,\eta} := \mathbf{W}_S^{1,h} + \operatorname{span}\left\{\delta_m^h \tilde{\mathbf{s}}_{m,n}\right\}_{n=1,m=1}^{N_m,M}. \tag{A.2}$$

Next we define a bound on the angle between the subspace spanned by the approximate singular basis functions at a given singular point $\mathbf{x}_m$ and the subspace $\mathbf{W}_S^1$. Let

$$\mathcal{S}_m(\eta, h) := \operatorname{span}\{\delta_m^h \tilde{\mathbf{s}}_{m,n}\}_{n=1}^{N_m}, \tag{A.3}$$

and let

$$\gamma_m(h) := \sup_{\eta \leq \eta_{m,0}} \sup_{\mathbf{s} \in \mathcal{S}_m, \mathbf{u} \in \mathbf{W}_S^1} \frac{\mathcal{F}^{nc}\langle \mathbf{s}, \mathbf{u}\rangle}{|\mathbf{s}|_{\mathbf{W}^h}|\mathbf{u}|_{\mathbf{W}^h}}. \tag{A.4}$$

This yields the following result.

LEMMA A.1 (strengthened Cauchy–Schwarz inequality). *For every singular point $\mathbf{x}_m$ there is a constant $\gamma_m(h) < 1.0$ such that*

$$\mathcal{F}^{nc}(\mathbf{s}, \mathbf{w}) \leq \gamma_m |\mathbf{s}|_{\mathbf{W}^h}|\mathbf{w}|_{\mathbf{W}^h} \tag{A.5}$$

for every $\mathbf{s} \in \mathcal{S}_m$ and $\mathbf{w} \in \mathbf{W}_S^1$.

Proof. For any fixed $h > 0, \eta > 0$, there is a positive angle between $\mathcal{S}_m$ and $\mathbf{W}_S^1$. Thus, $\gamma_m < 1.0$ ∎

This leads to the following bound.

LEMMA A.2. *Let $\mathbf{w} \in \mathbf{W}^{h,\eta}$ have the form*

$$\mathbf{w} = \sum_{m=1}^{M}\sum_{n=1}^{N_m} \beta_{m,n}\delta^m \tilde{\mathbf{s}}_{m,n} + \mathbf{w}_0^h, \tag{A.6}$$

where $\mathbf{w}_0^h \in \mathbf{W}_S^{1,h}$. Then

$$\sum_{m=1}^{M}\sum_{n=1}^{N_m} \beta_{m,n}^2 |\delta_m^h \tilde{\mathbf{s}}_{m,n}|_{\mathbf{W}^h}^2 \leq \frac{C}{1-\gamma^2}|\mathbf{w}|_{\mathbf{W}^h}^2, \tag{A.7}$$

where $\gamma = \max_m \gamma_m$.

Proof. The result follows from the fact that the singular basis functions associated with different singular points are mutually orthogonal and from the strengthened Cauchy–Schwarz inequality. For this proof only, let $\mathcal{P}_m$ represent the platform and fringe around singular point m.

$$\begin{aligned}
|\mathbf{w}|^2_{\mathbf{W}^h} &\geq \left|\sum_{i=1}^{M}\sum_{n=1}^{N-m} \beta_{m,n}\delta_m^h\tilde{\mathbf{s}}_{m,n}\right|^2_{\mathbf{W}^h} - 2\mathcal{F}\left\langle \sum_{i=1}^{M}\sum_{n=1}^{N_m} \beta_{m,n}\delta_m^h\tilde{\mathbf{s}}_{m,n},\ \mathbf{w}_0\right\rangle + |\mathbf{w}_0|^2_{\mathbf{W}^h} \\
&\geq \sum_{i=1}^{M}\left|\sum_{n=1}^{N_m} \beta_{m,n}\delta_m^h\tilde{\mathbf{s}}_{m,n}\right|^2_{\mathbf{W}^h} \\
&\quad - 2\sum_{i=1}^{M}\gamma_m\left|\sum_{n=1}^{N_m} \beta_{m,n}\delta_m^h\tilde{\mathbf{s}}_{m,n}\right|_{\mathbf{W}^h} |\mathbf{w}_0|_{\mathbf{W}^h,\mathcal{P}_m} + |\mathbf{w}_0|^2_{\mathbf{W}^h} \\
&\geq (1-\gamma^2)\sum_{i=1}^{M}\left|\sum_{n=1}^{N_m} \beta_{m,n}\delta_m^h\tilde{\mathbf{s}}_{m,n}\right|^2_{\mathbf{W}^h} + |\mathbf{w}_0|^2_{\mathbf{W}^h} - \sum_{m=1}^{M}|\mathbf{w}_0|^2_{\mathbf{W}^h,\mathcal{P}_m} \\
&\geq (1-\gamma^2)\sum_{i=1}^{M}\left|\sum_{n=1}^{N_m} \beta_{m,n}\delta_m^h\tilde{\mathbf{s}}_{m,n}\right|^2_{\mathbf{W}^h}.
\end{aligned}$$

Since the singular functions associated with any give singular point are linearly independent, there exists a constant C_m independent of h such that

$$\left|\sum_{n=1}^{N_m} \beta_{m,n}\delta_m^h\tilde{\mathbf{s}}_{m,n}\right|_{\mathbf{W}^h} \geq C_m \sum_{n=1}^{N_m}|\beta_{m,n}|^2 \left\|\delta_m^h\tilde{\mathbf{s}}_{m,n}\right\|^2_{\mathbf{W}^h}. \tag{A.8}$$

This completes the proof. ∎

We now show a Poincaré–Friedrichs inequality for the bilinear form. The nonconformity is rooted in the fact that the singular basis functions, $\delta_m^h\tilde{\mathbf{s}}_{m,n}$, do not satisfy the jump conditions exactly. Suppose that Γ_{ij} is the interface between Ω_I and Ω_J. Let $[g]_{\Gamma_{ij}}$ denote the jump in g across Γ_{ij} . Let $\mathbf{w} \in \mathbf{W}^{h,\eta}$ be defined as in (A.6). We have

$$\begin{aligned}
\left[\mathbf{n}\cdot\sqrt{a}\mathbf{w}\right]_{\Gamma_{ij}} &= \left[\mathbf{n}\cdot\sqrt{a}\sum_{m=1}^{M}\sum_{n=1}^{N_m} \beta_{m,n}\delta_m^h\tilde{\mathbf{s}}_{m,n}\right]_{\Gamma_{ij}} \\
&= \sum_{m\ :\ \Gamma_{ij}\cap\mathcal{P}_k\neq\emptyset}\ \sum_{n=1}^{N_m} \beta_{m,n}\left[\mathbf{n}\cdot\sqrt{a}\delta_m^h\tilde{\mathbf{s}}_{m,n}\right]_{\Gamma_{ij}}, \\
\left[\boldsymbol{\tau}\cdot\frac{1}{\sqrt{a}}\mathbf{w}\right]_{\Gamma_{ij}} &= \left[\boldsymbol{\tau}\cdot\frac{1}{\sqrt{a}}\sum_{m=1}^{M}\sum_{n=1}^{N_m} \beta_{m,n}\delta_m^h\tilde{\mathbf{s}}_{m,n}\right]_{\Gamma_{ij}} \\
&= \sum_{m\ :\ \Gamma_{ij}\cap\mathcal{P}_k\neq\emptyset}\ \sum_{n=1}^{N_m} \beta_{m,n}\left[\boldsymbol{\tau}\cdot\frac{1}{\sqrt{a}}\delta_m^h\tilde{\mathbf{s}}_{m,n}\right]_{\Gamma_{ij}}.
\end{aligned}$$

THEOREM A.3. *Let* γ *be defined as in Lemma* A.2. *Let* η *bound the maximum error in* $\tilde{\alpha}_{m,n}$, $\tilde{\lambda}_{m,n}$, *and* $\tilde{\mu}_{m,n}$. *Then, there exist constants* C_1 *and* C_2 *independent*

of h, η such that

$$\|\mathbf{u}\|_{0,\Omega} \le C\frac{\eta^2}{1-\gamma^2}\,|\mathbf{u}|_{\mathbf{W}^h} \tag{A.9}$$

for all $\mathbf{w} \in \mathbf{W}^{h,\eta}$.

Proof. Consider a Helmholtz decomposition on $\mathbf{W}^h$: for $\mathbf{u} \in \mathbf{W}^h$, there exist p, $\psi \in H^1(\Omega)$ such that

$$\mathbf{u} = \sqrt{a}\nabla p + \frac{1}{\sqrt{a}}\nabla^\perp \psi \tag{A.10}$$

where p is the unique solution of the weak equation

$$\begin{array}{rcll} \langle a\nabla p,\, \nabla q\rangle &=& \langle \sqrt{a}\mathbf{u},\, \nabla q\rangle\,, & \\ p = q &=& 0 & \text{on } \Gamma_D, \\ \mathbf{n}\cdot a\nabla p &=& 0 & \text{on } \Gamma_N, \end{array} \tag{A.11}$$

and ψ is the unique (up to a constant) solution of

$$\begin{array}{rl} \left\langle \dfrac{1}{a}\nabla^\perp\psi,\, \nabla^\perp\phi\right\rangle = \left\langle \dfrac{1}{\sqrt{a}}\mathbf{u},\, \nabla^\perp\phi\right\rangle, & \\ \psi = C_i,\, \phi = 0 & \text{on } \Gamma_{N_i}, \\ \mathbf{n}\cdot\dfrac{1}{a}\nabla\psi = 0 & \text{on } \Gamma_D, \end{array} \tag{A.12}$$

where C_i are arbitrary constants, one of which may be set to zero.

Note that the decomposition is orthogonal in the L^2 sense:

$$\left\langle \sqrt{a}\nabla p,\, \frac{1}{\sqrt{a}}\nabla^\perp\psi\right\rangle_{0,\Omega} = 0. \tag{A.13}$$

We thus have

$$\|\mathbf{u}\|^2_{0,\Omega} = \left\|\sqrt{a}\nabla p\right\|^2_{0,\Omega} + \left\|\frac{1}{\sqrt{a}}\nabla^\perp\psi\right\|^2_{0,\Omega}. \tag{A.14}$$

This next step uses the fact that the jump conditions across boundaries are satisfied exactly except for the singular basis functions, which have support only on $\mathcal{P}_m$ for $m = 1, \ldots, M$.

We assume that a is a constant on $\mathcal{P}_m \cap \Omega_i$ and that $\Gamma_{ij} \cap \mathcal{P}_k$ is a straight line starting from the singular point, $\mathbf{x}_m$. We have

$$\begin{aligned} \left\|\sqrt{a}\nabla p\right\|^2_{0,\Omega} &= \left\langle \sqrt{a}\nabla p,\, \sqrt{a}\nabla p\right\rangle_{0,\Omega} = \sum_{i=1}^{J}\langle a\nabla p,\, \nabla p\rangle_{0,\Omega_i} \\ &= \sum_{i=1}^{J}\left\langle -\nabla\cdot\sqrt{a}\mathbf{u},\, p\right\rangle_{0,\Omega_i} + \oint_{\partial\Omega_i}\left(\mathbf{n}\cdot\sqrt{a}\mathbf{u}\right)p \\ &= \sum_{i=1}^{J}\left\langle -\frac{1}{\sqrt{a}}\nabla\cdot\sqrt{a}\mathbf{u},\, \sqrt{a}p\right\rangle_{0,\Omega_i} + \sum_{ij}\int_{\Gamma_{ij}}\left[\mathbf{n}\cdot\sqrt{a}\mathbf{u}\right]p \\ &\le \sum_{i=1}^{J}\left\|\frac{1}{\sqrt{a}}\nabla\cdot\sqrt{a}\mathbf{u}\right\|_{0,\Omega_i}\left\|\sqrt{a}p\right\|_{0,\Omega_i} \\ &\quad + \left|\sum_{ij}\sum_{m:\Gamma_{ij}\cap\mathcal{P}_m\neq\emptyset}\int_{\Gamma_{ij}\cap\mathcal{P}_m}\sum_{n=1}^{N_m}\beta_{m,n}\left[\mathbf{n}\cdot\sqrt{a}\delta^h_m\tilde{\mathbf{s}}_{m,n}\right]p\right|. \end{aligned}$$

With our assumptions, we have

$$\begin{aligned}
&\int_{\Gamma_{ij}\cap\mathcal{P}_m} \sum_{n=1}^{N_m} \beta_{m,n} \left[\mathbf{n}\cdot\sqrt{a}\delta_m^h \tilde{\mathbf{s}}_{m,n}\right] p \\
&\leq C_m\eta \sum_{n=1}^{N_m} |\beta_{m,n}| \left| \int_0^{R_m} \delta_m^h(r) r^{(\tilde{\alpha}_n-1)} p(r) dr \right| \\
&\leq C_m\eta \sum_{n=1}^{N_m} |\beta_{m,n}| \left(\left\|\sqrt{a}_i p\right\|_{1/2,\Gamma_{ij}\cap\mathcal{P}_k} + \left\|\sqrt{a}_j p\right\|_{1/2,\Gamma_{ij}\cap\mathcal{P}_m} \right),
\end{aligned}$$

where R_m is the radius of $\mathcal{P}_m$. Here C_m involves $\min_\Omega |a|$.

Plugging this into the expression above, after first using the ϵ-inequality twice, and using a trace inequality $\|\sqrt{a}p\|_{1/2,\partial(\Omega_i\cap\mathcal{P}_k)} \leq C\|\sqrt{a}\nabla p\|_{0,\Omega_i\cap\mathcal{P}_k}$, the fact that $\|\frac{1}{\sqrt{a}}\nabla\cdot\sqrt{a}\delta_k^h\tilde{\mathbf{s}}_k^\eta\|_{0,\mathcal{P}_k} \leq C$, where C is independent of h and η, and the Poincaré–Friedrichs inequality on p in [2, Lemma 3.1], we get

$$\begin{aligned}
&\left\|\sqrt{a}\nabla p\right\|_{0,\Omega}^2 \\
&\leq \sum_{i=1}^{J} \left\| \frac{1}{\sqrt{a}}\nabla\cdot\sqrt{a}\mathbf{u} \right\|_{0,\Omega_i} \left\|\sqrt{a}p\right\|_{0,\Omega_i} \\
&\quad + \sum_{ij} \sum_{m:\Gamma_{ij}\cap\mathcal{P}_m\neq\emptyset} C_m\eta \sum_{n=1}^{N_m} |\beta_{M,n}| \left(\left\|\sqrt{a}_i p\right\|_{1/2,\Gamma_{ij}\cap\mathcal{P}_m} + \left\|\sqrt{a}_j p\right\|_{1/2,\Gamma_{ij}\cap\mathcal{P}_m} \right) \\
&\leq \frac{1}{\epsilon_1}\sum_{i=1}^{J} \left\| \frac{1}{\sqrt{a}}\nabla\cdot\sqrt{a}\mathbf{u} \right\|_{0,\Omega_i}^2 + \epsilon_1 \left\|\sqrt{a}p\right\|_{0,\Omega_i}^2 + \frac{1}{\epsilon_2}\sum_m C_m^2\eta^2 \sum_{n=1}^{N_m} |\beta_{m,n}|^2 \\
&\quad + 2\epsilon_2 \sum_{ij} \sum_{m:\Gamma_{ij}\cap\mathcal{P}_m\neq\emptyset} \left(\left\|\sqrt{a}_i p\right\|_{1/2,\Gamma_{ij}\cap\mathcal{P}_m}^2 + \left\|\sqrt{a}_j p\right\|_{1/2,\Gamma_{ij}\cap\mathcal{P}_m}^2 \right) \\
&\leq \frac{1}{\epsilon_1}\sum_{i=1}^{J} \left\| \frac{1}{\sqrt{a}}\nabla\cdot\sqrt{a}\mathbf{u} \right\|_{0,\Omega_i}^2 + \epsilon_1 c_4 \left\|\sqrt{a}\nabla p\right\|_{0,\Omega_i}^2 \\
&\quad + \frac{C\eta^2}{\epsilon_2}\sum_{i=1}^{J} \sum_{k:\Omega_i\cap\mathcal{P}_k\neq\emptyset} \sum_{n=1}^{N_m} |\beta_{m,n}|^2 \left\| \frac{1}{\sqrt{a}}\nabla\cdot\sqrt{a}\delta_m^h\tilde{\mathbf{s}}_{m,n} \right\|_{0,\Omega_i\cap\mathcal{P}_m}^2 + 2C_1\epsilon_2 \left\|\sqrt{a}\nabla p\right\|_{0,\Omega_i}^2 .
\end{aligned}$$

Choosing appropriate ϵ_1 and ϵ_2 yields

$$\begin{aligned}
\left\|\sqrt{a}\nabla p\right\|_{0,\Omega}^2 \leq C \Bigg(&\sum_{i=1}^{J} \left\| \frac{1}{\sqrt{a}}\nabla\cdot\sqrt{a}\mathbf{u} \right\|_{0,\Omega_i}^2 \\
&+ \eta^2 \sum_i \sum_{m:\Omega_i\cap\mathcal{P}_m\neq\emptyset} \sum_{n=1}^{N_m} |\beta_{m,n}|^2 \left\| \frac{1}{\sqrt{a}}\nabla\cdot\sqrt{a}\delta_m^h\tilde{\mathbf{s}}_{m,n} \right\|_{0,\Omega_i\cap\mathcal{P}_m}^2 \Bigg).
\end{aligned} \tag{A.15}$$

A similar result follows for the other term in the decomposition,

$$\left\|\frac{1}{\sqrt{a}}\nabla^{\perp}\psi\right\|_{0,\Omega}^{2} \le C\left(\sum_{i=1}^{J}\left\|\sqrt{a}\nabla\times\frac{1}{\sqrt{a}}\mathbf{u}\right\|_{0,\Omega_i}^{2} + \eta^{2}\sum_{i}\sum_{m:\Omega_i\cap\mathcal{P}_m\neq\emptyset}\sum_{n=1}^{N_m}|\beta_{m,n}|^{2}\left\|\sqrt{a}\nabla\times\frac{1}{\sqrt{a}}\delta_m^h\tilde{\mathbf{s}}_{m,n}\right\|_{0,\Omega_i\cap\mathcal{P}_m}^{2}\right). \tag{A.16}$$

Putting (A.15) and (A.16) together and applying Lemma A.2 yields

$$\begin{aligned}\|\mathbf{u}\|_{0,\Omega}^{2} &= \left\|\sqrt{a}\nabla p\right\|_{0,\Omega}^{2} + \left\|\frac{1}{\sqrt{a}}\nabla^{\perp}\psi\right\|_{0,\Omega}^{2} \\ &\le C|\mathbf{u}|_{\mathbf{W}^h}^{2} + C\eta^{2}\sum_{m}\sum_{n=1}^{N_m}|\beta_{m,n}|^{2}|\delta_m^h\tilde{\mathbf{s}}_{m,n}|_{\mathbf{W}^h}^{2} \\ &\le \left(C_1 + \frac{C_2\eta^{2}}{(1-\gamma^{2})}\right)|\mathbf{u}|_{\mathbf{W}^h}^{2}.\end{aligned} \tag{A.17}$$

This completes the proof. ∎

COROLLARY A.4. *Under the assumption $\gamma = 1 - O(h^2)$, there are constant $C1$ and C_2, independent of h, such that*

$$\|\mathbf{u}\|_{0,\Omega}^{2} \le \left(C_1 + C_2\frac{\eta^{2}}{h^{2}}\right)|\mathbf{u}|_{\mathbf{W}^h}. \tag{A.18}$$

Proof. The proof follows immediately from Theorem A.3. ∎

To eliminate h-dependence, we must ensure that $\eta = O(h)$. Recall that η is the error in the exponent of the singular basis function. In our numerical scheme for the calculation of the exponents, we have full control over their accuracy.

REFERENCES

[1] A. E. BERGER, L. R. SCOTT, AND G. STRANG, *Approximate boundary conditions in the finite element method*, Sympos. Math., 10 (1972), pp. 295–313.

[2] M. BERNDT, T. A. MANTEUFFEL, S. F. MCCORMICK, AND G. STARKE, *Analysis of first-order system least squares (FOSLS) for elliptic problems with discontinuous coefficients: Part* I, SIAM J. Numer. Anal., 43 (2005), pp. 386–408.

[3] P. BOCHEV, Z. CAI, T. A. MANTEUFFEL, AND S. F. MCCORMICK, *Analysis of velocity-flux first-order system least-squares principles for the Navier–Stokes equations: Part* I, SIAM J. Numer. Anal., 35 (1998), pp. 990–1009.

[4] P. B. BOCHEV AND M. D. GUNZBURGER, *Finite element methods of least-squares type*, SIAM Rev., 40 (1998), pp. 789–837.

[5] J. H. BRAMBLE, R. D. LAZAROV, AND J. E. PASCIAK, *A least-squares approach based on a discrete minus one inner product for first order systems*, Math. Comp., 66 (1997), pp. 935–955.

[6] J. H. BRAMBLE AND J. E. PASCIAC, *Least-squares methods for the Stokes equations based on a discrete minus one inner product*, J. Comput. Appl. Math., 74 (1996), pp. 155–173.

[7] S. C. BRENNER, *Multigrid methods for the computation of singular solutions and stress intensity factors* I: *Corner singularities*, Math. Comput., 68 (1999), pp. 559–583.

[8] S. C. BRENNER AND L. R. SCOTT, *The Mathematical Theory of Finite Elements*, Springer-Verlag, New York, Berlin, 1994.

[9] S. C. BRENNER AND L. Y. SUNG, *Multigrid methods for the computation of singular solutions and stress intensity factors* II: *Crack singularities*, BIT, 37 (1997), pp. 623–643.

[10] Z. Cai and S. Kim, *A finite element method using singular functions for the Poisson equation: Corner singularities*, SIAM J. Numer. Anal., 39 (2001), pp. 286–299.
[11] Z. Cai, R. Lazarov, T. A. Manteuffel, and S. F. McCormick, *First-order system least squares for second-order partial differential equations: Part* I, SIAM J. Numer. Anal., 31 (1994), pp. 1785–1799.
[12] Z. Cai, T. A. Manteuffel, and S. F. McCormick, *First-order system least squares for second-order partial differential equations: Part* II, SIAM J. Numer. Anal., 34 (1997), pp. 425–454.
[13] Z. Cai, T. A. Manteuffel, and S. F. McCormick, *First-order system least squares for the Stokes equations, with application to linear elasticity*, SIAM J. Numer. Anal., 34 (1997), pp. 1727–1741.
[14] Z. Cai, T. A. Manteuffel, S. F. McCormick, and J. Ruge, *First-order system LL* (FOSLL*): Scalar elliptic partial differential equations*, SIAM J. Numer. Anal., 39 (2001), pp. 1418–1445.
[15] T. F. Chen and G. J. Fix, *Least squares finite element simulation of transonic flows*, Appl. Numer. Math., 2 (1986), pp. 399–408.
[16] P. G. Ciarlet and J. L. Lions, *Finite Element Methods (Part* 1*)*, North–Holland, Amsterdam, 1990.
[17] C. L. Cox and G. J. Fix, *On the accuracy of least squares methods in the presence of corner singularities*, Comput. Math. Appl., 10 (1984), pp. 463–475.
[18] G. Fix and E. Stephan, *Finite Element Methods of the Least Squares Type for Regions with Corners*, Tech. Report 81-41, Institute for Computer Applications in Science and Engineering (ICASE), NASA Langley Research Center, Hampton, VA, 1981.
[19] P. Grisvard, *Elliptic Problems in Nonsmooth Domains*, Pitman, Boston, 1985.
[20] D. C. Jespersen, *A least-square decomposition method for solving elliptic systems*, Math. Comp., 31 (1977), pp. 873–880.
[21] B. N. Jiang and J. Z. Chai, *Least-squares finite element analysis of steady high subsonic plane potential flows*, Acta Mech. Sinica, 1 (1980), pp. 90–93 (in Chinese).
[22] B.-N. Jiang and C. L. Chang, *Least-squares finite elements for the Stokes problem*, Comput. Methods Appl. Mech. Engrg., 78 (1990), pp. 297–311.
[23] R. B. Kellogg, *Singularities in interface problems*, in Proceedings of the 2nd Symposium on Numerical Solution of Partial Differential Equations (SYNSPADE 1970), University of Maryland, 1971, pp. 351–400.
[24] T. A. Manteuffel, S. F. McCormick, and G. Starke, *Analysis of first-order system least squares (FOSLS) for elliptic problems with discontinuous coefficients*, in Proceedings of the Seventh Copper Mountain Conference on Multigrid Methods, NASA Conference Publication 3339, NASA, Washington, DC, 1996, pp. 535–550.
[25] P. Neittaanmäki and J. Saranen, *On finite element approximation of the gradient for the solution to Poisson equation*, Numer. Math., 37 (1981), pp. 131–148.
[26] A. I. Pehlivanov and G. F. Carey, *Error estimates for least-squares mixed finite elements*, RAIRO Modél. Math. Anal. Numér., 28 (1994), pp. 499–516.
[27] A. I. Pehlivanov, G. F. Carey, and R. D. Lazarov, *Least-squares mixed finite elements for second-order elliptic problems*, SIAM J. Numer. Anal., 31 (1994), pp. 1368–1377.
[28] U. Rüde, *On the accurate computation of singular solutions of Laplace's and Poisson's equation*, Multigrid Methods: Theory, Applications, and Supercomputing, 110 (1988), pp. 517–540.
[29] J. Ruge and K. Stüben, *Efficient solution of finite difference and finite element equations by algebraic multigrid (amg)*, in Multigrid Methods for Integral and Differential Equations, D. J. Paddon and H. Holstein, eds., Inst. Math. Appl. Conf. Ser. New Ser. 3, Oxford University Press, New York, 1985, pp. 169–212.
[30] G. Strang and G. J. Fix, *An Analysis of the Finite Element Method*, Prentice-Hall, Englewood Cliffs, NJ, 1973.
[31] K. Stüben and U. Trottenberg, *Multigrid methods: Fundamental algorithms, model problem analysis and applications*, in Multigrid Methods, W. Hackbusch and U. Trottenberg, eds., Lecture Notes in Math. 960, Springer–Verlag, Berlin, 1982, pp. 1–176.
[32] W. L. Wendland, *Elliptic Systems in the Plane*, Pitman, London, 1979.
[33] E. Zauderer, *Partial Differential Equations of Applied Mathematics*, 2nd ed., Ser. Pure Appl. Math., John Wiley & Sons, New York, 1988.